nature

https://doi.org/10.1038/s41586-021-04186-8

Accelerated Article Preview

Pre-existing polymerase-specific T cells expand in abortive seronegative SARS-CoV-2

Received: 17 June 2021

Accepted: 27 October 2021

Accelerated Article Preview Published online 10 November 2021

Cite this article as: Swadling, L. et al. Pre-existing polymerase-specific T cells expand in abortive seronegative SARS-CoV-2. *Nature* https://doi.org/10.1038/s41586-021-04186-8 (2021).

Leo Swadling, Mariana O. Diniz, Nathalie M. Schmidt, Oliver E. Amin, Aneesh Chandran, Emily Shaw, Corinna Pade, Joseph M. Gibbons, Nina Le Bert, Anthony T. Tan, Anna Jeffery-Smith, Cedric C. S. Tan, Christine Y. L. Tham, Stephanie Kucykowicz, Gloryanne Aidoo-Micah, Joshua Rosenheim, Jessica Davies, Marina Johnson, Melanie P. Jensen, George Joy, Laura E. McCoy, Ana M. Valdes, Benjamin M. Chain, David Goldblatt, Daniel M. Altmann, Rosemary J. Boyton, Charlotte Manisty, Thomas A. Treibel, James C. Moon, COVIDsortium investigators, Lucy van Dorp, Francois Balloux, Áine McKnight, Mahdad Noursadeghi, Antonio Bertoletti & Mala K. Maini

Article

Pre-existing polymerase-specific T cells expand in abortive seronegative SARS-CoV-2

https://doi.org/10.1038/s41586-021-04186-8

Received: 17 June 2021

Accepted: 27 October 2021

Published online: 10 November 2021

Leo Swadling[1]✉, Mariana O. Diniz[1,24], Nathalie M. Schmidt[1,24], Oliver E. Amin[1,24], Aneesh Chandran[1,24], Emily Shaw[1,24], Corinna Pade[2], Joseph M. Gibbons[2], Nina Le Bert[3], Anthony T. Tan[3], Anna Jeffery-Smith[1,2], Cedric C. S. Tan[4], Christine Y. L. Tham[3], Stephanie Kucykowicz[1], Gloryanne Aidoo-Micah[1], Joshua Rosenheim[1], Jessica Davies[1], Marina Johnson[5], Melanie P. Jensen[6,7], George Joy[6,8], Laura E. McCoy[1], Ana M. Valdes[9,10], Benjamin M. Chain[1], David Goldblatt[5], Daniel M. Altmann[11], Rosemary J. Boyton[12,13], Charlotte Manisty[6,8], Thomas A. Treibel[6,8], James C. Moon[6,8], COVIDsortium investigators*, Lucy van Dorp[4], Francois Balloux[4], Áine McKnight[2], Mahdad Noursadeghi[1,24], Antonio Bertoletti[3,14,24] & Mala K. Maini[1]✉

Individuals with potential exposure to SARS-CoV-2 do not necessarily develop PCR or antibody positivity, suggesting some may clear sub-clinical infection before seroconversion. T-cells can contribute to the rapid clearance of SARS-CoV-2 and other coronavirus infections[1–3]. We hypothesised that pre-existing memory T-cell responses, with cross-protective potential against SARS-CoV-2[4–11], would expand *in vivo* to support rapid viral control, aborting infection. We measured SARS-CoV-2-reactive T-cells, including those against the early transcribed replication transcription complex (RTC)[12,13], in intensively monitored healthcare workers (HCW) remaining repeatedly negative by PCR, antibody binding, and neutralisation (seronegative HCW, SN-HCW). SN-HCW had stronger, more multispecific memory T-cells than an unexposed pre-pandemic cohort, and more frequently directed against the RTC than the structural protein-dominated responses seen post-detectable infection (matched concurrent cohort). SN-HCW with the strongest RTC-specific T-cells had an increase in IFI27, a robust early innate signature of SARS-CoV-2[14], suggesting abortive infection. RNA-polymerase within RTC was the largest region of high sequence conservation across human seasonal coronaviruses (HCoV) and SARS-CoV-2 clades. RNA-polymerase was preferentially targeted (amongst regions tested) by T-cells from pre-pandemic cohorts and SN-HCW. RTC epitope-specific T-cells cross-recognising HCoV variants were identified in SN-HCW. Enriched pre-existing RNA-polymerase-specific T-cells expanded *in vivo* to preferentially accumulate in the memory response after putative abortive compared to overt SARS-CoV-2 infection. Our data highlight RTC-specific T-cells as targets for vaccines against endemic and emerging *Coronaviridae*.

There is wide variability in the outcome of exposure to SARS-CoV-2, ranging from severe illness to asymptomatic infection, to those remaining negative with standard diagnostic tests. Recent studies have identified SARS-CoV-2 T-cell reactivity in pre-pandemic samples[5–11,15–18] and isolated cases of exposed individuals who have not seroconverted with single time point screening[4,16,19–22]. We studied an intensively monitored cohort of HCW with potential exposure during the first UK pandemic wave, comparing those with or without PCR and/or antibody evidence of SARS-CoV-2 infection. We postulated that in HCW where PCR, and the most sensitive binding and neutralising antibody (nAb) tests, remained repeatedly negative (SN-HCW), T-cell assays might distinguish a subset with a subclinical, rapidly

[1]Division of Infection and Immunity, University College London, London, UK. [2]Blizard Institute, Barts and the London School of Medicine and Dentistry, Queen Mary University of London, London, UK. [3]Emerging Infectious Diseases Program, Duke-NUS Medical School, Singapore, Singapore. [4]UCL Genetics Institute, University College London, London, UK. [5]Great Ormond Street Institute of Child Health NIHR Biomedical Research Centre, University College London, London, UK. [6]Barts Heart Centre, St Bartholomew's Hospital, Barts Health NHS Trust, London, UK. [7]Department of Cellular Pathology, Northwest London Pathology, Imperial College London NHS Trust, London, UK. [8]Institute of Cardiovascular Science, University College London, London, UK. [9]Academic Rheumatology, Clinical Sciences, Nottingham City Hospital, Nottingham, UK. [10]NIHR Nottingham Biomedical Research Centre, Nottingham University Hospitals NHS Trust and University of Nottingham, Nottingham, UK. [11]Department of Immunology and Inflammation, Imperial College London, London, UK. [12]Department of Infectious Disease, Faculty of Medicine, Imperial College London, London, UK. [13]Lung Division, Royal Brompton & Harefield Hospitals, Guy's and St. Thomas' NHS Foundation Trust, London, UK. [14]Singapore Immunology Network, A*STAR, Singapore, Singapore. [24]These authors contributed equally: Mariana O. Diniz, Nathalie M. Schmidt, Oliver E. Amin, Aneesh Chandran, Emily Shaw, Mahdad Noursadeghi, Antonio Bertoletti. *A list of authors and their affiliations appears at the end of the paper. ✉e-mail: l.swadling@ucl.ac.uk; m.maini@ucl.ac.uk

terminated (abortive) infection. We hypothesised that these individuals would exhibit pre-existing memory T-cells with cross-reactive potential, obviating the time required for *de novo* before, or at the time of, potential exposure.

We included analysis of the understudied T-cells directed against the core RTC within open reading frame (ORF)1ab (RNA-polymerase co-factor non-structural protein 7 [NSP7], RNA-polymerase NSP12, and helicase NSP13, henceforth referred to as RTC); these are putative targets for pre-existing responses with pan-*Coronaviridae* reactivity, because they are likely to be highly conserved due to their key early roles in the viral life cycle. Consistent with this, where immunity against other viruses (including HBV, HCV, HIV and JEV) has been described in exposed seronegative individuals, T-cells were noted to be more likely to target non-structural proteins, such as polymerase, than in those with seropositive infection[23–27].

SARS-CoV-2 T-cells in seronegative HCW

We compared T-cell reactivity in intensively monitored infected or SN-HCW, matched for exposure risk and demographic factors (COVIDsortium, Extended Data Table 1, Fig. 1a). Additional control cohorts comprised healthy adults sampled in London, UK or Singapore prior to SARS-CoV-2 circulation in humans (pre-pandemic cohort; Fig. 1a). SN-HCW were defined by negative weekly diagnostic tests (baseline-wk16, SARS-CoV-2 PCR, nasopharyngeal swab; anti-Spike-1 IgG and anti-nucleoprotein [NP] IgG/IgM seroassays[28], Fig. 1b-d). Having previously reported a range of nAb titres at wk16 in laboratory-confirmed infection, we examined nAb in SN-HCW. Two HCW with nAb titres just above the threshold were excluded from further analyses; the remaining SN-HCW were negative by pseudotype assay (Fig. 1e), with a subset also confirmed negative at three time points for authentic virus neutralisation (Extended Data Fig. 1a). SN-HCW could have become PCR negative by recruitment, however, non-seroconverters after PCR positivity were rare (2.6% of PCR+ HCW negative by all 3 seroassays[16]) and antibody responses are unlikely to have waned before recruitment[28]. Furthermore, SN-HCW lacked detectable SARS-CoV-2 spike-specific memory B-cells, which we have shown persist after waning of nAb[29] (Extended Data Fig. 1b, below detection threshold). Thus, SN-HCW represented a cohort of intensely monitored HCW who resisted classical laboratory-confirmed infection.

We quantified SARS-CoV-2-specific memory T-cells by ELISpot using unbiased stimulation with overlapping peptides covering structural proteins and the less well-studied non-structural proteins of the RTC (Fig. 1f). As previously described, when using sensitive assays[5–7,9,17,18] (e.g. 400,000 PBMC/well IFNγ-ELISpot used here[8,16]), some SARS-CoV-2-reactive T-cells were detectable in pre-pandemic samples; however, their multispecificity was significantly lower than in the wk16 laboratory-confirmed infection group (Fig. 1g-h; structural responses at wk16 previously reported[16]). By contrast, SN-HCW had SARS-CoV-2-specific T-cells comparable in breadth to infected HCW at wk16 and significantly more multispecific than pre-pandemic samples (Fig. 1g-h). SN-HCW targeted more protein pools and had a ~5-fold higher cumulative magnitude of responses, than pre-pandemics, with an overall strength equivalent to the infected cohort at wk16 (Fig. 1i-j).

T-cells from pre-pandemic samples tended not to target both halves of NP (NP1 & NP2 subpools), whereas around 50% of SN-HCW and laboratory-confirmed infection group did, confirming our earlier suggestion[8] that this serves as a simple proxy-measure of a multispecific response (Extended Data Fig. 1c-e). Taken together, we found a higher magnitude and breadth of SARS-CoV-2-specific T-cells in repeatedly PCR and antibody negative HCW than in a pre-pandemic cohort.

RTC-specific T-cells and IFI27 in SN-HCW

We next asked whether T-cell memory differs in SN-HCW versus HCW with laboratory-confirmed infection. Anti-viral T-cells recognising Influenza A (flu), Epstein-Barr virus (EBV) and cytomegalovirus (CMV) (FEC) were equivalent between the three cohorts (Extended Data Fig. 2a). However, the relative immunodominance of T-cells against SARS-CoV-2 structural versus RTC proteins differed between groups. The laboratory-confirmed infection group had more responses to structural proteins (Spike, Membrane, NP, and ORF3a) than to RTC (NSP7, NSP12, NSP13) (Fig. 2a-b). Memory T-cells against structural proteins tended to positively correlate with viral load, whereas RTC responses did not show this association (Extended Data Fig. 2b). By contrast, SN-HCW targeted both structural and RTC regions, with significantly more RTC-specific T-cells than either the infected or pre-pandemic groups (Fig.2a, Extended Data Fig. 2c-d). Pre-pandemic samples had a ratio of RTC to structural responses that did not differ significantly from that in SN-HCW (Fig.2b), pointing to a possible influence of pre-existing responses on the pool of T-cells expanding in SN-HCW. A further small group (10%) of HCW had PCR-confirmed infection but lacked detectable nAb at wk16, some of whom also lacked binding antibodies; interestingly this sub-group was similarly enriched for RTC-reactive T-cells (Extended Data Fig. 2e-f). Taken together, this suggests that the structural proteins, abundantly produced during active infection, are dominant T-cell targets after mild infection, whereas T-cells in SN-HCW preferentially focus on the RTC.

To confirm the T-cell identity of ELISpot responses in SN-HCW at wk16 we expanded them with RTC peptides and detected both CD4+ and CD8+ SARS-CoV-2-specific T-cells dividing (CTV dilution) and producing IFNγ (Extended Data Fig. 3a; Extended Data Table 2). Their post-expansion frequencies tended to be lower than control flu/EBV/CMV-specific responses in the same donors but proportional to their differing *ex vivo* frequencies, indicating comparable proliferative potential (Extended Data Fig. 3b). *In vitro* expanded RTC-specific T-cells in SN-HCW were also highly functional, producing multiple cytokines in tandem (Extended Data Fig. 3c-d). Most of the SARS-CoV-2-specific T-cells expanded from SN-HCW were CD4+, however, CD8+ T-cells were also detectable in the majority of individuals (Extended Data Fig. 3e).

Our data raised the possibility that SARS-CoV-2 infection in HCW represents a spectrum, with some SN-HCW expanding T-cells as a result of sub-clinical infection not detectable by PCR or antibody seroconversion. To test this postulate, we measured the interferon-inducible transcript IFI27 in blood, which we recently showed detects SARS-CoV-2 infection at, or one week before, PCR positivity (specificity 0.95 and sensitivity 0.84[14]). Of the 25% of SN-HCW with the strongest post-exposure RTC-specific T-cell responses (Extended Data Fig. 4a), 40% (i.e. 10% of SN-HCW group) already had IFI27 levels at recruitment that were above the threshold set on a cohort of unexposed pre-pandemic samples, although their levels tended to be lower than in laboratory-confirmed infection (Fig. 2c). To further estimate the frequency of abortive infections we tested a larger cohort of 99 unselected SN-HCW baseline samples, finding a comparable proportion (9.1%) had IFI27 induction above the pre-pandemic threshold (Fig. 2c). IFI27 signal peaked above the pre-pandemic threshold in 93.3% of those with strong RTC-specific T-cells over wk0-5, but in none with weak or undetectable RTC-specific T-cells (Fig. 2c). IFI27 levels showed a cumulative increase, peaking at 3-5 weeks post-UK lockdown (Fig. 2d, by which time all first wave laboratory-confirmed infections had occurred Fig. 1b). By contrast IFI27 was unchanged over wk0-5 in SN-HCW with weak or absent RTC-specific responses, resulting in lower IFI27 slope and variance (Fig. 2d, Extended Data Fig. 4b-c). Peak IFI27 level correlated with NSP7 T-cells at wk16, with the latter correlating more strongly with NSP12 and other RTC-specific than structural responses. Neither IFI27 or T-cell specificity correlated with age, sex, or other demographic factors, such as exposure type, in this small cohort (Extended Data Fig. 4d, Extended Data Table 1).

In summary, during a period of high transmission at the start of the first UK pandemic wave, a low-level systemic interferon response indicative of virus exposure was detectable selectively in individuals who had the strongest SARS-CoV-2-specific T-cells post-exposure, despite them lacking PCR or antibody confirmation of infection. Extrapolating from our previous data showing that IFI27 is induced at the time of incident infection and correlates with viral load[14], this is consistent with low-level infection among SN-HCW with stronger RTC-specific T-cell responses.

Targeting of conserved RNA-polymerase

A transient/abortive infection not detectable by PCR or seroconversion could conceivably result from a lower viral inoculum and/or from a more efficient innate and/or adaptive immune response. The latter would be favoured by pre-existing memory T-cells with the potential to expand rapidly upon cross-recognition of early viral products of SARS-CoV-2 replication. Early T-cell proliferation and T-cell receptor clonal expansion, even prior to detectable virus, has been observed during mild SARS-CoV-2 infection[17,30] and expansion of virus-specific T-cells predates antibody induction after mRNA vaccination[2,31]. Having found the SN-HCW group to be enriched for SARS-CoV-2-specific T-cells, particularly against RTC, we investigated the possibility that some of these represented expansions of pre-existing cross-reactive responses.

Likely candidates for the source of pre-existing T-cells that cross-recognise SARS-CoV-2 are previous infections with closely related human endemic common cold coronaviruses (α-HCoV 229E, NL63, and β-HCoV HKU1, OC43). We bioinformatically determined the sequence homology of all possible SARS-CoV-2-derived 15mer peptides to a curated set of HCoV sequences (Supplementary Table 1). RTC proteins, expressed at the first stage of the SARS-CoV-2 life cycle[13], had 15mer sequences of high homology to HCoV (Fig. 3a)[32,33]. In particular, NSP7, NSP12, and NSP13-derived 15mers had 6.3, 29.9 and 31.0% higher average sequence homology to the four HCoV species compared to structural protein-derived 15mers (all $p<0.001$, Fig. 3b). NSP12 being the largest of these proteins, represented the region with the most homology overall amongst human-infecting *Coronaviridae*. We further assessed diversity across global circulating SARS-CoV-2 sequences (13,785 representative sub-sample of 611,893 sequences, GISAID, 27th July 2021; Extended Data Fig. 5a) using Nei's genetic diversity index and an estimate of the minimal number of independent mutational events (homoplasies) at any nucleotide. By both metrics, RTC proteins NSP12 and NSP13 were among the most conserved across SARS-CoV-2 clades (Fig.3c, Extended Data Fig. 5b-d) and were significantly more conserved than many structural proteins (Extended Data Table 3).

Importantly, the highly conserved RNA-polymerase (NSP12) was also the region amongst those tested in pre-pandemic samples that was most commonly targeted by T-cells, with the highest average magnitude and frequency of responders (Fig. 3d). Of note, the same preferential targeting of NSP12 was observed in a geographically distinct cohort of pre-pandemic samples from Singapore (Fig. 3d). Pre-existing T-cells had the potential to recognise all viral antigens tested, including those with less conservation across HCoV, as previously described[5,7,17,34]. Responses against these regions were further enriched in SN-HCW (Fig. 3d-e; Mann-Whitney $p<0.0001$ for all except ORF3a $p=0.0006$, NSP13 $p=0.0003$), suggesting many sources of pre-existing and *de novo* responses contribute to T-cell memory in exposed seronegative individuals. Despite potential demographic confounders between cohorts (Extended Data Table 1), as with pre-pandemics samples, SN-HCW preferentially targeted NSP12 (Fig. 3e). Therefore, the viral protein most commonly targeted by pre-existing T-cells is also the largest conserved region between *coronaviridae*, suggesting exposure to HCoV is one likely source of cross-reactive T-cells.

To further explore the potential for cross-reactivity due to prior infection with seasonal HCoV, we mapped novel and previously described[6,8,18,35] RTC-specific CD4+ and CD8+ T-cell epitopes in SN-HCW, revealing high sequence conservation with HCoV (Extended Data Table 4; Extended Data Fig. 6a-b). We identified cross-reactivity against the HLA-A*02:01 restricted epitope in NSP7. A subset of T-cells co-stained with MHC class I pentamers loaded with SARS-CoV-2 and HKU1 sequence peptide *ex vivo*, and bound SARS-CoV-2 peptide-loaded pentamer after 10-day expansion with either peptide (Extended Data Fig. 6c). T-cells from 3/5 HLA-A*02:01+ SN-HCW tested had stronger responses to the HKU1 sequence than to other seasonal HCoV or SARS-CoV-2 (Extended Data Fig. 6d-e). This suggested prior HKU1 infection primed these NSP7 responses that are able to cross-recognise the SARS-CoV-2 sequence, albeit with reduced efficiency. HLA-B*35+ SN-HCW also showed variable cross-recognition of seasonal HCoV variant sequences of an NSP12 epitope (Extended Data Fig. 6f).

An alternative explanation for expanded T-cells with cross-reactive potential in SN-HCW is an infection with a seasonal coronavirus during the first wave of SARS-CoV-2 infections in London. As expected, all HCW had detectable anti-spike IgG against the 4 endemic HCoV and, as previously described[36], spike-specific antibodies against β-coronavirus OC43 were boosted in those with PCR detectable infection and SARS-CoV-2-specific seroconversion (Extended Data Fig. 7). However, there was no difference in endemic HCoV titres in HCW who had strong RTC-specific T-cells and raised IFI27 compared to those with weak or absent RTC-specific responses (Extended Data Fig. 7), making it unlikely that HCoV infection itself accounted for the SARS-CoV-2-reactive T-cells we detected in SN-HCW.

In summary, RTC regions like polymerase, expressed in the first stage of the viral life cycle, are highly conserved among HCoV and are preferentially targeted by T-cells in pre-pandemic and SN-HCW samples. A subset of T-cells from donors able to abort infection could cross-recognise SARS-CoV-2 and HCoV sequences at individual RTC epitopes, pointing to prior infection with HCoV as one source of pre-existing cross-reactive T-cells.

Polymerase T-cells in abortive infection

To examine whether pre-existing cross-reactive and/or rapidly generated *de novo* RTC-specific T-cells expand *in vivo*, we obtained paired PBMC samples pre- and post-SARS-CoV-2 exposure. Medical students and laboratory staff (Contact Cohort, n = 23) sampled prior to the COVID-19 pandemic (winter 2018-2019), were re-sampled after close contact with infected cases, with or without IgG seroconversion +/- PCR positivity (Contact Cohort, Extended Data Table 5). Parallel analysis of pre- and post-exposure/infection PBMC demonstrated expansion of RTC over structural responses in the close-contact seronegative group (Fig. 4a). By contrast, the group with serological confirmation of infection showed the expected *in vivo* expansion of pre-existing structural SARS-CoV-2-reactive T-cells, with no significant increase in RTC-specific T-cells (Fig. 4a; Extended Data Fig. 8a). We observed *in vivo* expansion of pre-existing NSP12 responses in 4/5 individuals who remained seronegative after exposure to SARS-CoV-2, resulting in a significant increase in NSP12 but not control Flu/EBV/CMV responses (Extended Data Fig. 8b-c). 4/5 remaining seronegative close contacts had newly detected, presumed *de novo*, low-level responses after exposure (Extended Data Fig. 8c).

We then reverted to the SN-HCW group, where small volume PBMC collections were available from the time of recruitment, allowing targeted analysis of baseline T-cells in those with the strongest RTC responses at wk16. NSP12-specific T-cells were already detectable at baseline in 79% of those SN-HCW with the strongest NSP12 responses post-exposure (Fig. 4b). NSP12 responses expanded *in vivo* on average 8.4-fold between recruitment and wk16, with no corresponding change in Flu/EBV/CMV responses (Fig. 4c, Extended Data Fig. 8d). We confirmed the expansion at wk16 of pre-existing RTC-specific T-cells at the level of subpool (Extended Data Fig. 8e-f) and individual peptide

(Fig. 4c, Extended Data Fig. 8g). In addition, many T-cells were newly detected post-exposure (Extended Data Fig. 8g), reflecting either *de novo* priming or expansion of responses previously below the limit of assay detection (example of expanded response undetectable by *ex vivo* ELISpot, Extended Data Fig. 8h). All HCW with newly detected or expanding/contracting NSP12-specific T-cells had both NP1 and NP2-reactive T-cells after exposure (Extended Data Fig. 8i), whereas only 2/5 with no change in NSP12 had these specificities, suggesting they may not have had the same level of SARS-CoV-2 exposure. The fold-change in NSP12 between recruitment and wk16 follow-up correlated with the total SARS-CoV-2 response, supporting its utility to identify seronegative individuals expanding T-cell immunity after exposure (Extended Data Fig. 8j).

Finally, we examined whether there was a preferential enrichment of RTC-specific responses in SN-HCW compared to the laboratory-confirmed infected HCW at wk16. Strikingly, the RNA-polymerase NSP12 and its cofactor NSP7 were the only proteins inducing higher magnitude T-cell responses in seronegative individuals in whom detectable infection was not established compared to those with overt infection (Fig. 4d). T-cells in SN-HCW targeted a larger number of regions of NSP12 (subpools of ~40 overlapping 15mers, Fig. 1g) than those in pre-pandemic or seropositive cohorts (Extended Data Fig. 8k). T-cells targeting several regions of NSP12 and other RTC pools were enriched in SN-HCW compared to laboratory-confirmed infection (Fig. 4d, lower panel). To examine whether the reduced frequency of NSP12-specific T-cells in the 16wk memory response of those with laboratory-confirmed infection was reflective of their repertoire at the time of encountering SARS-CoV-2, we obtained baseline PBMC from a subset sampled prior to PCR positivity or >4wks before seroconversion. NSP12-specific T-cells were already significantly lower at baseline in those that went on to develop laboratory-confirmed infection than in SN-HCW (Fig. 4e, Extended Data Fig. 8l-m), supporting a potential role in protection from PCR-detectable infection and seroconversion.

Conclusions

We provide T-cell and innate transcript evidence for abortive, seronegative SARS-CoV-2 infection. Longitudinal samples from SN-HCW and an additional cohort, showed RTC (particularly polymerase)-specific T-cells were enriched before exposure, expanded *in vivo*, and preferentially accumulated in those in whom SARS-CoV-2 failed to establish infection, compared to those with overt infection.

The differential biasing of T-cells towards early expressed non-structural SARS-CoV-2 proteins in HCW not seroconverting may reflect repetitive occupational exposure to very low viral inocula, reported to drive the induction of non-structural T-cells in HIV, SIV and HBV[26,37,38]. Such repetitive exposure would be congruent with the observed protracted induction of the innate signal IFI27 and the development of *de novo* T-cells in some SN-HCW.

However, we also documented expansion of pre-existing T-cells, with responses capable of cross-recognising epitope variants between seasonal HCoV and SARS-CoV-2. Cross-reactive SARS-CoV-2-specifc CD8+ T-cells directed against epitopes highly conserved among HCoV are now well-described, with pre-existing T-cells frequently targeting essential viral proteins with low scope for tolerating mutational variation, such as those in ORF1ab[6,18,32]. The abundant SARS-CoV-2-specific CD4+ T-cells may also contribute to protection in SN-HCW by antibody-independent mechanisms, such as antiviral cytokines and chemokines production. HCW have higher frequencies of HCoV-reactive T-cells than the general public[19] and recent HCoV infection is associated with reduced risk of severe COVID-19 infection[39], likely partly attributable to cross-reactive neutralising antibodies;[40,41] however, pre-existing T-cells have also been implicated[15,42]. The early induction of T-cells, before detectable antibodies in mild infection[30] and concurrent with mRNA vaccination efficacy, support a role for pre-existing cross-reactive memory T-cells[2,31].

Pre-existing RTC-specific T-cells, at higher frequency than naïve T-cells and poised for immediate re-activation on antigen cross-recognition, would be expected to favour early control, explaining their enrichment after abortive compared to classical infection. However, the relative contribution of viral inoculum and cross-reactive T-cells needs to be further dissected in human challenge experiments and animal models. A caveat of this work is that we only analysed peripheral immunity; it is plausible that mucosal-sequestered antibodies[43] played a role in our seronegative cohort. It also remains possible that innate immunity mediates control in abortive infections, with RTC-biased T-cell responses being generated as a biomarker of low-grade infection. Interferon-independent induction of RIG-I has been proposed to abort SARS-CoV-2 infection by restraining the viral lifecycle prior to sgRNA production;[13] this would favour the presentation of epitopes from ORF1ab, released into the cytoplasm in the first stage of the viral life cycle[12], whilst blocking production of structural proteins from pgRNA. This raises the possibility that some SARS-CoV-2 infected cells could be recognised and removed by ORF1ab-reactive T-cells without widespread production of structural proteins and mature virion formation.

We have described induction of innate and cellular immunity without seroconversion, highlighting a subset of individuals where risk of SARS-CoV-2 reinfection and immunogenicity of vaccines should be specifically assessed. The HCW we studied were exposed to Wuhan Hu-1 and had partial protection from PPE; it remains to be seen whether abortive infections can occur upon exposure to more infectious variants of concern, or in the presence of vaccine-induced immunity. However, clearance without seroconversion points to T-cells which may be particularly effective vaccine targets. Cross-protection between coronaviruses is proportional to their sequence homology in mice[44], making the highly conserved NSP12 region studied here, as well as less studied NSP3/14/16, top candidates for heterologous immunity. Our data highlight the presence of pre-existing T-cells in a proportion of donors that are able to expand *in vivo* and target a highly conserved region of SARS-CoV-2 and other *Coronaviridae*. Boosting of such T-cells may offer durable pan-*Coronaviridae* reactivity against endemic and emerging viruses, arguing for their inclusion and assessment, as an adjunct to spike-specific antibodies, in next-generation vaccines.

Online content

Any methods, additional references, Nature Research reporting summaries, source data, extended data, supplementary information, acknowledgements, peer review information; details of author contributions and competing interests; and statements of data and code availability are available at https://doi.org/10.1038/s41586-021-04186-8.

1. Tan, A. T. et al. Early induction of functional SARS-CoV-2-specific T cells associates with rapid viral clearance and mild disease in COVID-19 patients. *Cell Rep.* **34**, 108728 (2021).
2. Oberhardt, V. et al. Rapid and stable mobilization of CD8+ T cells by SARS-CoV-2 mRNA vaccine. *Nature* (2021) https://doi.org/10.1038/s41586-021-03841-4.
3. Zhao, J. J. et al. Airway Memory CD4+ T Cells Mediate Protective Immunity against Emerging Respiratory *Coronaviruses*. *Immunity* **44**, 1379–1391 (2016).
4. Sekine, T. et al. Robust T Cell Immunity in Convalescent Individuals with Asymptomatic or Mild COVID-19. *Cell* **183**, 158-168.e14 (2020).
5. Mateus, J. et al. Selective and cross-reactive SARS-CoV-2 T cell epitopes in unexposed humans. *Science (80-.).* **370**, 89–94 (2020).
6. Nelde, A. et al. SARS-CoV-2-derived peptides define heterologous and COVID-19-induced T cell recognition. *Nat. Immunol.* **22**, 74–85 (2021).
7. Braun, J. et al. SARS-CoV-2-reactive T cells in healthy donors and patients with COVID-19. *Nature* **587**, 270–274 (2020).
8. Le Bert, N. et al. SARS-CoV-2-specific T cell immunity in cases of COVID-19 and SARS, and uninfected controls. *Nature* **584**, 457–462 (2020).
9. Grifoni, A. et al. Targets of T Cell Responses to SARS-CoV-2 Coronavirus in Humans with COVID-19 Disease and Unexposed Individuals. *Cell* **181**, 1489-1501.e15 (2020).
10. Schulien, I. et al. Characterization of pre-existing and induced SARS-CoV-2-specific CD8+ T cells. *Nat. Med.* **27**, 78–85 (2021).
11. Loyal, L. et al. Cross-reactive CD4 $^{+}$ T cells enhance SARS-CoV-2 immune responses upon infection and vaccination. *Science (80-.).* eabh1823 (2021) https://doi.org/10.1126/SCIENCE.ABH1823.

12. Perlman, S. & Netland, J. Coronaviruses post-SARS: Update on replication and pathogenesis. *Nat. Rev. Microbiol.* **7**, 439–450 (2009).
13. Yamada, T. et al. RIG-I triggers a signaling-abortive anti-SARS-CoV-2 defense in human lung cells. *Nat. Immunol.* (2021) https://doi.org/10.1038/s41590-021-00942-0.
14. Gupta, R. K. et al. Blood transcriptional biomarkers of acute viral infection for detection of pre-symptomatic SARS-CoV-2 infection. *medRxiv* 2021.01.18.21250044 (2021) https://doi.org/10.1101/2021.01.18.21250044.
15. Mallajosyula, V. et al. CD8+ T cells specific for conserved coronavirus epitopes correlate with milder disease in COVID-19 patients. *Sci. Immunol.* **6**, 1–27 (2021).
16. Reynolds, C. J. et al. Discordant neutralizing antibody and T cell responses in asymptomatic and mild SARS-CoV-2 infection. *Sci. Immunol.* **5**, (2020).
17. Low, J. S. et al. Clonal analysis of immunodominance and cross-reactivity of the CD4 T cell response to SARS-CoV-2. *Science (80-.).* eabg8985 (2021) https://doi.org/10.1126/science.abg8985.
18. Ferretti, A. P. et al. Unbiased Screens Show CD8+ T Cells of COVID-19 Patients Recognize Shared Epitopes in SARS-CoV-2 that Largely Reside outside the Spike Protein. *Immunity* **53**, 1095-1107.e3 (2020).
19. da Silva Antunes, R. et al. Differential T cell reactivity to endemic coronaviruses and SARS-CoV-2 in community and health care workers. *J. Infect. Dis.* **2021**.01.12.21249683 (2021) https://doi.org/10.1093/infdis/jiab176.
20. Wang, Z. et al. Exposure to SARS-CoV-2 generates T-cell memory in the absence of a detectable viral infection. *Nat. Commun.* **12**, 1724 (2021).
21. Ogbe, A. et al. T cell assays differentiate clinical and subclinical SARS-CoV-2 infections from cross-reactive antiviral responses. *Nat. Commun.* **12**, (2021).
22. Gallais, F. et al. Intrafamilial exposure to SARS-CoV-2 associated with cellular immune response without Seroconversion, France. *Emerg. Infect. Dis.* **27**, 113–121 (2021).
23. Wiegand, J. et al. HBV-specific T-cell responses in healthy seronegative sexual partners of patients with chronic HBV infection. *J. Viral Hepat.* **17**, 631–639 (2010).
24. Promadej, N. et al. Broad human immunodeficiency virus (HIV)-specific T cell responses to conserved HIV proteins in HIV-seronegative women highly exposed to a single HIV-infected partner (Journal of Infectious Diseases (2003) 187 (1053-1063)). *J. Infect. Dis.* **187**, 1346 (2003).
25. Heller, T. et al. Occupational exposure to hepatitis C virus: Early T-cell responses in the absence of seroconversion in a longitudinal cohort study. *J. Infect. Dis.* **208**, 1020–1025 (2013).
26. Rowland-Jones, S. et al. HIV-specific cytotoxic T-cells in HIV-exposed but uninfected Gambian women. *Nat. Med.* **1**, 59–64 (1995).
27. Turtle, L. et al. Human T cell responses to Japanese encephalitis virus in health and disease. *J. Exp. Med.* **213**, 1331–1352 (2016).
28. Manisty, C. et al. Time series analysis and mechanistic modelling of heterogeneity and sero-reversion in antibody responses to mild SARS-CoV-2 infection. *EBioMedicine* **65**, 103259 (2021).
29. Jeffery-Smith, A. et al. SARS-CoV-2-specific memory B cells can persist in the elderly despite loss of neutralising 1 antibodies 2 3 4. *bioRxiv* 2021.05.30.446322 (2021) https://doi.org/10.1101/2021.05.30.446322.
30. Chandran, A. et al. Title Non-severe SARS-CoV-2 infection is characterised by very early T cell proliferation independent of type 1 interferon responses and distinct from other acute respiratory viruses. *medRxiv* 2021.03.30.21254540 (2021) https://doi.org/10.1101/2021.03.30.21254540.
31. Kalimuddin, S. et al. Early T cell and binding antibody responses are associated with COVID-19 RNA vaccine efficacy onset. *Med* **0**, 1–7 (2021).
32. Tan, C. C. S. et al. Pre-existing T cell-mediated cross-reactivity to SARS-CoV-2 cannot solely be explained by prior exposure to endemic human coronaviruses 2 3. *bioRxiv* 2020.12.08.415703 (2020).
33. Buckley, P. R., Lee, C. H., Pinho, M. P. & Babu, R. O. HLA-dependent variation in SARS-CoV-2 CD8 + T cell cross- reactivity with human coronaviruses. (2021).
34. Nelde, A. et al. SARS-CoV-2 T-cell epitopes define heterologous and COVID-19-induced T-cell recognition. (2020) https://doi.org/10.21203/rs.3.rs-35331/v1.
35. Grifoni, A. et al. SARS-CoV-2 human T cell epitopes: Adaptive immune response against COVID-19. *Cell Host Microbe* **29**, 1076–1092 (2021).
36. Anderson, E. M. et al. Seasonal human coronavirus antibodies are boosted upon SARS-CoV-2 infection but not associated with protection. *Cell* **184**, 1858-1864.e10 (2021).
37. Clerici, M. et al. T-cell proliferation to subinfectious SIV correlates with lack of infection after challenge of macaques. *Aids* vol. 8 1391–1395 (1994).
38. Werner, J. M., Abdalla, A., Gara, N., Ghany, M. G. & Rehermann, B. The hepatitis B vaccine protects re-exposed health care workers, but does not provide sterilizing immunity. *Gastroenterology* **145**, 1026–1034 (2013).
39. Sagar, M. et al. Recent endemic coronavirus infection is associated with less-severe COVID-19. *J. Clin. Invest.* **131**, (2021).
40. Ng, K. W. et al. Preexisting and de novo humoral immunity to SARS-CoV-2 in humans. *Science (80-.).* **370**, 1339–1343 (2020).
41. Yang, F. et al. Shared B cell memory to coronaviruses and other pathogens varies in human age groups and tissues. *Science (80-.).* **372**, 738–741 (2021).
42. Wyllie, D. et al. SARS-CoV-2 responsive T cell numbers are associated with protection from COVID-19: A prospective cohort study in keyworkers. *medRxiv* (2020) https://doi.org/10.1101/2020.11.02.20222778.
43. Cervia, C. et al. Systemic and mucosal antibody responses specific to SARS-CoV-2 during mild versus severe COVID-19. *J. Allergy Clin. Immunol.* **147**, 545-557.e9 (2021).
44. Dangi, T. et al. SARS coronavirus vaccines protect against different coronaviruses. *bioRxiv* 2021.06.01.446491 (2021).

COVIDsortium investigators

Hakam Abbass[6], Aderonke Abiodun[6,8], Mashael Alfarih[6], Zoe Alldis[6], Daniel M. Altmann[11], Oliver E. Amin[1,24], Mervyn Andiapen[6], Jessica Artico[6], João B. Augusto[6], Georgina L. Baca[6], Sasha N. L. Bailey[12], Anish N. Bhuva[6], Alex Boulter[6], Ruth Bowles[6], Rosemary J. Boyton[12], Olivia V. Bracken[15], Ben O'Brien[6,23], Tim Brooks[16], Natalie Bullock[2], David K. Butler[12], Gabriella Captur[17,8], Nicola Champion[6], Carmen Chan[6], Aneesh Chandran[1,24], David Collier[21], Jorge Couto de Sousa[6], Xose Couto-Parada[6], Teresa Cutino-Moguel[6], Rhodri H. Davies[6], Brooke Douglas[17], Cecilia Di Genova[18], Keenan Dieobi-Anene[6], Mariana O. Diniz[1,24], Anaya Ellis[16], Karen Feehan[15], Malcolm Finlay[6], Marianna Fontana[17], Nasim Forooghi[6], Celia Gaier[15], Joseph M. Gibbons[2], Derek Gilroy[19], Matt Hamblin[6], Gabrielle Harker[16], Jacqueline Hewson[16], Lauren M. Hickling[20], Aroon D. Hingorani[1], Lee Howes[8], Alun Hughes[8], Gemma Hughes[6], Rebecca Hughes[6,8], Ivie Itua[6], Victor Jardim[6], Wing-Yiu Jason Lee[2], Melanie petra Jensen[6], Jessica Jones[16], Meleri Jones[2], George Joy[6], Vikas Kapil[6,21], Hibba Kurdi[6,8], Jonathan Lambourne[6], Kai-Min Lin[12], Sarah Louth[17], Mala K. Maini[1], Vineela Mandadapu[6], Charlotte Manisty[6,8], Aine McKnight[2], Katia Menacho[6], Celina Mfuko[6], Oliver Mitchelmore[6], Christopher Moon[16], James C. Moon[6,8], Sam M. Murray[12], Mahdad Noursadeghi[1], Ashley Otter[16], Corinna Pade[2], Susana Palma[6], Ruth Parker[22], Kush Patel[6], Babita Pawarova[17], Steffen E. Petersen[6], Brian Piniera[6], Franziska P. Pieper[12], Daniel Pope[6,21], Mary Prossora[6], Lisa Rannigan[17], Alicja Rapala[8], Catherine J. Reynolds[12], Amy Richards[6], Matthew Robathan[21], Joshua Rosenheim[1], Genine Sambile[6], Nathalie M. Schmidt[1,24], Amanda Semper[16], Andreas Seraphim[6], Mihaela Simion[17], Angelique Smit[17], Michelle Sugimoto[15], Leo Swadling[1], Stephen Taylor[16], Nigel Temperton[18], Stephen Thomas[16], George D. Thornton[6,8], Thomas A. Treibel[6,8], Art Tucker[6], Jessry Veerapen[6], Mohit Vijayakumar[6], Sophie Welch[6], Theresa Wodehouse[6], Lucinda Wynne[6] & Dan Zahedi[22]

[15]Division of Medicine, University College London, London, UK. [16]National Infection Service, Public Health England, Porton Down, UK. [17]Royal Free London NHS Foundation Trust, London, UK. [18]Viral Pseudotype Unit, Medway School of Pharmacy, Chatham Maritime, Kent, UK. [19]Centre for Clinical Pharmacology, University College London, London, UK. [20]East London NHS Foundation Trust Unit for Social and Community Psychiatry, Newham Centre for Mental Health, London, UK. [21]William Harvey Research Institute, Queen Mary University of London, London, UK. [22]School of Clinical Medicine, University of Cambridge, Cambridge, UK. [23]German Heart Centre and Charité University, Berlin, Germany.

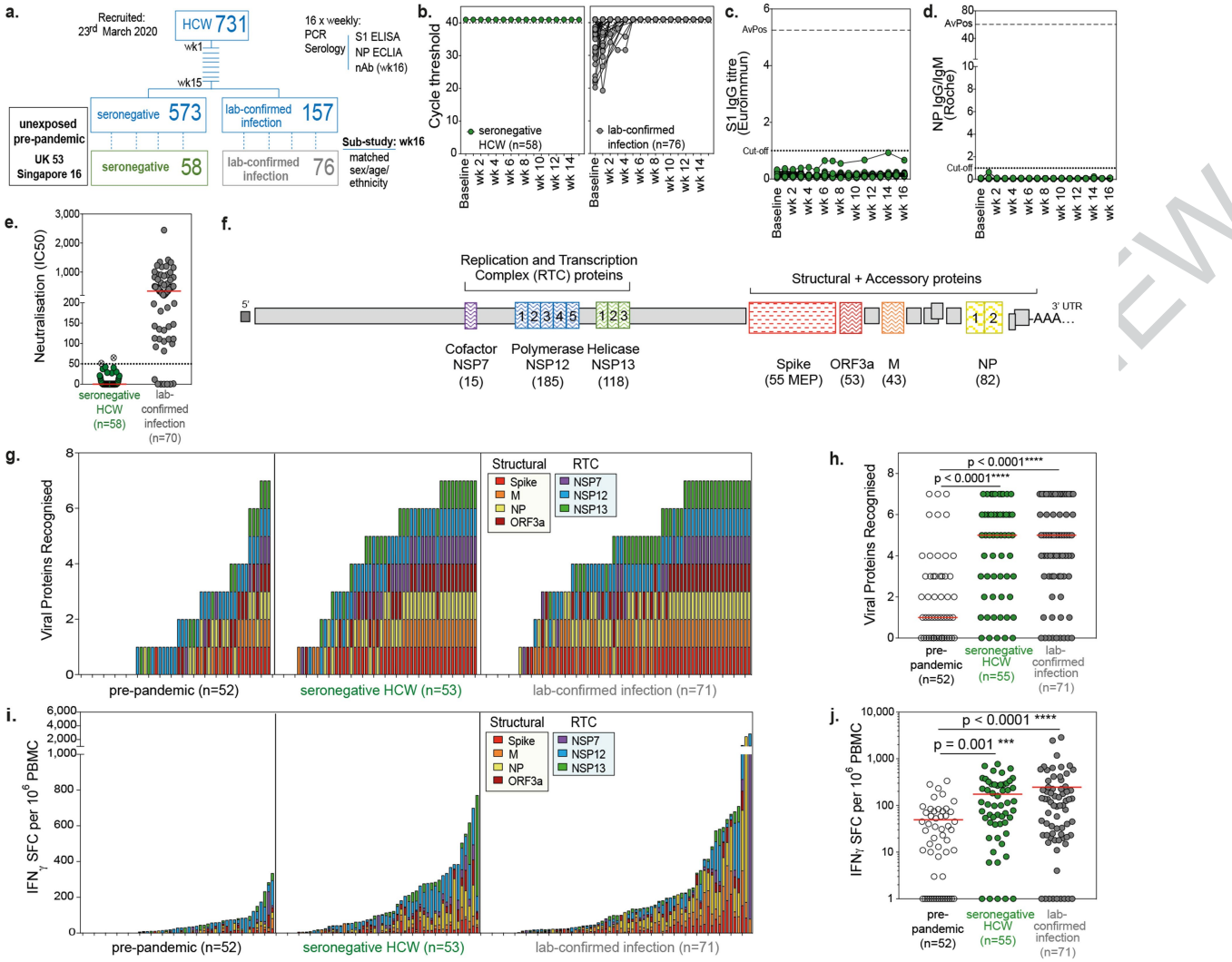

Fig. 1 | SARS-CoV-2-specific T-cells in seronegative HCW. a, Design of HCW and pre-pandemic cohorts. **b**, Cycle threshold values for E gene PCR in SN-HCW and laboratory-confirmed infection (undetectable at 40 cycles assigned 41). **c**, Anti-Spike S1 and **d**, anti-NP antibody titres in SN-HCW (baseline to wk16; n=58; dotted lines at assay positivity cut-off and at average peak [AvPos] response in laboratory-confirmed infection). **e**, Pseudovirus neutralisation at wk16. Crossed circles excluded from SN-HCW group (IC50 >50). **f**, SARS-CoV-2 proteome highlighting RTC and structural regions assayed for T-cell responses (peptide subpools identified by numbered boxes) and the number of overlapping 15mer peptides (or mapped epitope peptides [MEP] for spike) in brackets below. **g**, Viral proteins recognised by individuals coloured by specificity and **h**, number of viral proteins targeted by group. **i**, Magnitude of T-cell response coloured by viral protein and **j**, cumulative magnitude of T-cell response by group. Red bar, geomean. **g-j**, IFNγ-ELISpot. **e,h**, Red bar, median. **h,j**, Kruskal-Wallis with Dunn's correction. M, membrane; NP, nucleoprotein; RTC, replication-transcription complex; SFC, spot forming cells. **b-e,g-j**, COVIDsortium HCW cohort.

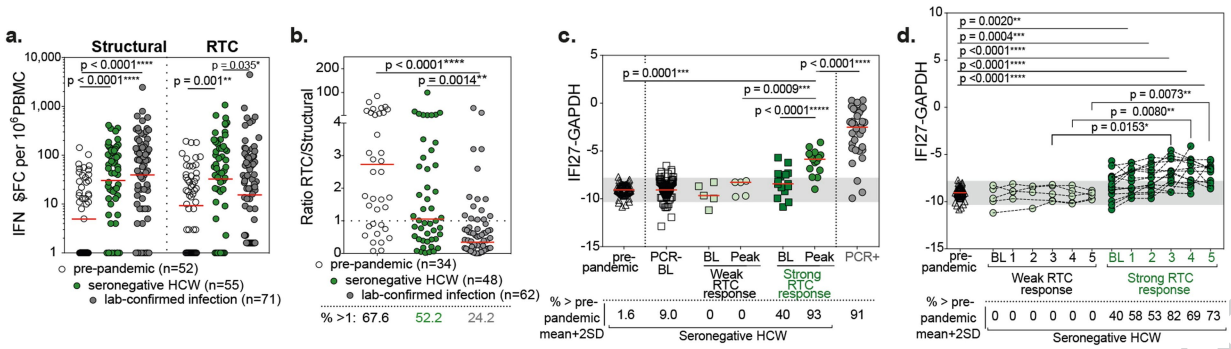

Fig. 2 | RTC-specific T-cell and IFI27 signature in SN-HCW. a, Magnitude of T-cell response to structural regions and RTC. **b**, Ratio of T-cell response to RTC versus structural regions. Percentage of cohort with a ratio above 1 (RTC>Structural) shown below. **c**, IFI27 transcript signal by RT-PCR in unexposed pre-pandemic samples (n=59), baseline samples in HCW that remained PCR- and seronegative throughout follow-up (n=99), SN-HCW with weak (n=5, <50 SFC/10^6 PBMC, Extended Data Fig. 4a) or strong (n=15, >50 SFC/10^6 PBMC) RTC-specific T-cells (baseline [BL] and peak signal [wk0-5]), and HCW at the time of PCR positivity (PCR+). **d**, longitudinal IFI27 signal in SN-HCW with weak or strong RTC-specific T-cell responses (n as in **c**). **c,d**, 2 standard deviations (SD) either side of the pre-pandemic cohort mean highlighted by grey area and percentage with raised IFI27 above mean+2SD indicated below. **a-b**, IFNγ-ELISpot. **a-b**, Red bar, geomean. **c-d**, Red bar, median. **a-d**, Kruskal-Wallis ANOVA with Dunn's correction. **c**, Mann-Whitney paired t-test. **a-b**, wk16. **a-d**, COVIDsortium HCW cohort.

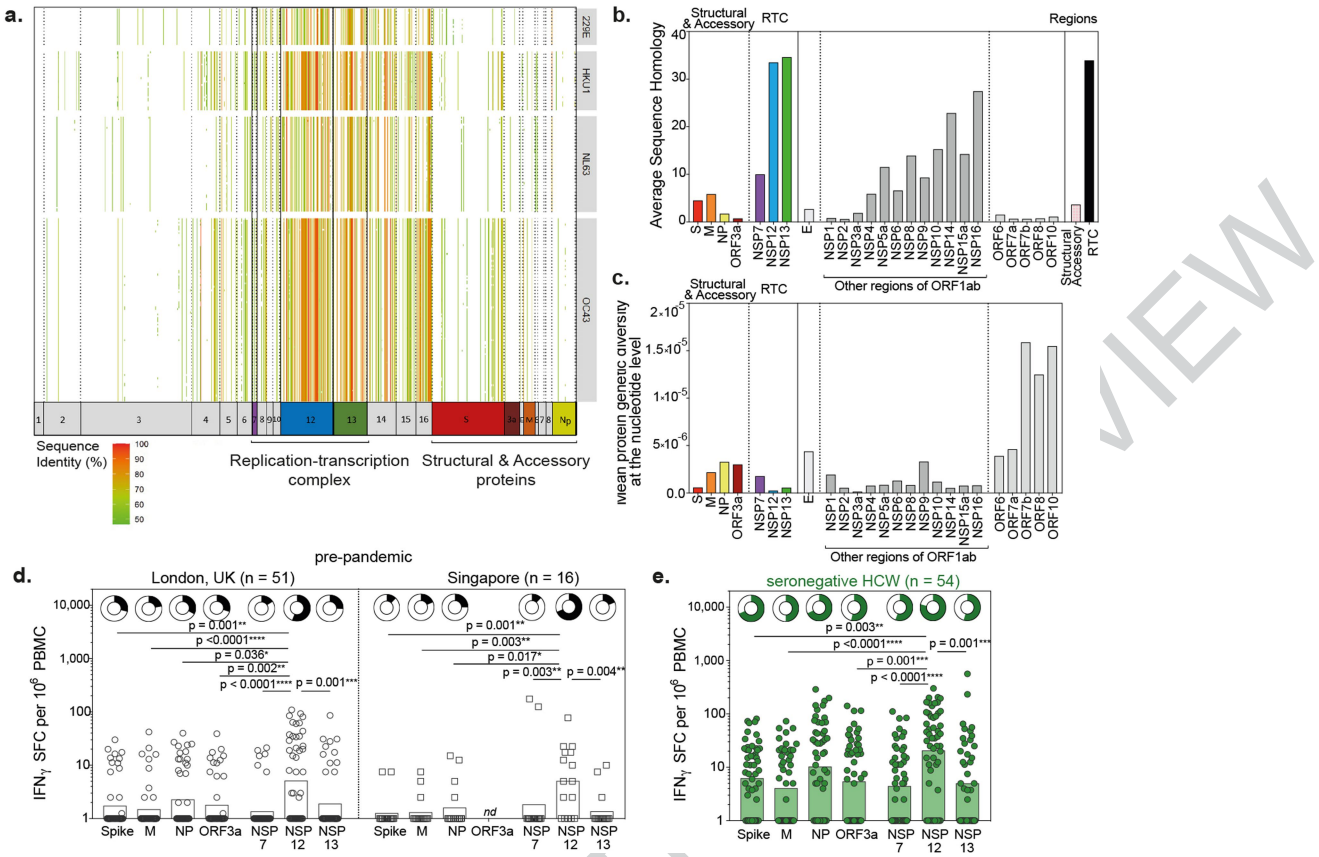

Fig. 3 | Cross-reactive T-cells targeting conserved RNA-polymerase. **a**, Heatmap, sequence homology of SARS-CoV-2-derived peptide sequences to HCoV sequences. Columns, 15mer SARS-CoV-2-derived peptides. Rows, HCoV genome records. Cells are coloured by the level of homology of the 15mer to a particular HCoV proteome. Heatmap cells with no fill indicate sequence homology <40% was observed. **b**, Average sequence homology of 15mers covering SARS-CoV-2 proteins, or regions (pink, structural [S, M, NP, ORF3a]; black, RTC [NSP7, NSP12, NSP13]), to HCoV sequences. Viral proteins not assayed for T-cell responses are shown in grey. **c**, Nucleotide diversity along the SARS-CoV-2 genome estimated with Nei's genetic diversity index, across each viral protein for all SARS-CoV-2 clades (subsampling Extended Data Fig. 5a). **d**, Magnitude of T-cell responses to individual SARS-CoV-2 proteins in unexposed pre-pandemic samples and **e**, SN-HCW at wk16. Frequency of responders shown as doughnuts above. **d-e**, IFNγ-ELISpot, bar at geomean. nd, not done. **d,e** Kruskal-Wallis with Dunn's correction. **d-e**, COVIDsortium HCW cohort.

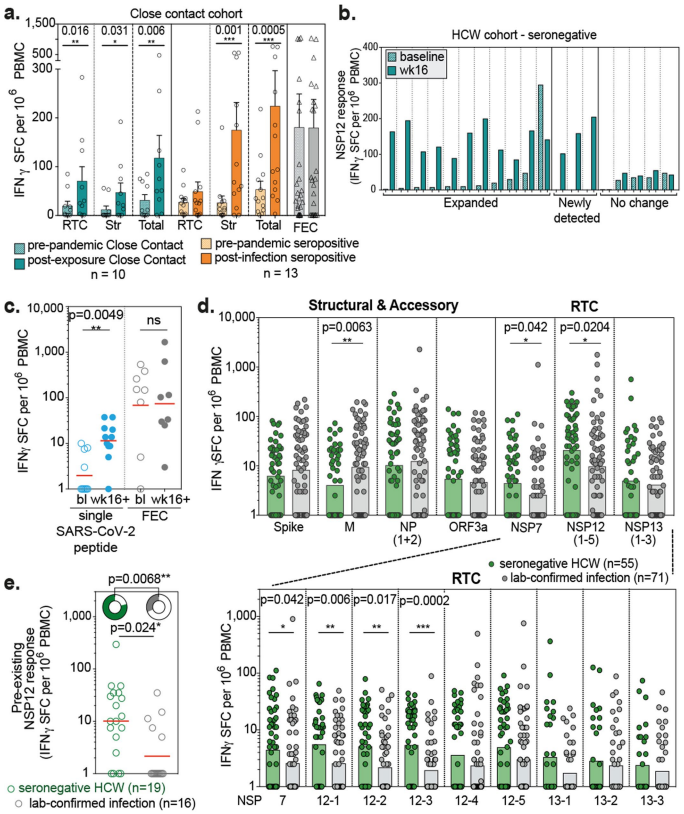

Fig. 4 | *In vivo* expansion of polymerase-specific T-cells in abortive infection. a, Magnitude of T-cell response in seronegative close contacts of cases (green), or in seropositive infected individuals (orange) to RTC, structural proteins, summed total, and Flu, EBV, CMV (FEC) peptide pool (grey seronegative/seropositive combined), before and after exposure/infection. Bar, mean + SEM. **b**, Change in magnitude of NSP12 T-cell response between recruitment and post-exposure in SN-HCW (sub-group with top 19 RTC responses at wk16, Extended Data Fig. 4a). Expanded, >2-fold change. **c**, Magnitude of paired pre- and post-exposure T-cell responses to individual 9-15mer peptides (individual responses Extended Data Fig. 8g) from RTC or control FEC pool in SN-HCW (wk16-26, 11 responses from 9 SN-HCW). **d**, Magnitude of T-cell response to individual SARS-CoV-2 proteins (upper panel) and to subpools (~40 overlapping peptides; lower panel) within RTC at wk16 in laboratory-confirmed infected HCW or SN-HCW. **e**, Pre-existing NSP12-specific T-cell responses in baseline samples from SN-HCW and laboratory-confirmed infection group (PCR+ after baseline or seroconversion at least 4 weeks post-recruitment). Doughnut plot above shows frequency. **a-e**, IFNγ-ELISpot. **c, d-e** Red line/bars, geomean. **a,c** Wilcoxon test. **d,e**, Mann-Whitney test and Fisher's exact test. **a**, Contact cohort, Extended Data Table 5. **b-e**, COVIDsortium HCW cohort, Extended Data Table 1).

Methods

COVIDsortium Healthcare Worker Participants

The COVIDsortium bioresource was approved by the ethical committee of UK National Research Ethics Service (20/SC/0149) and registered on ClinicalTrials.gov (NCT04318314). Full study details of the bioresource (participant screening, study design, sample collection, and sample processing) have been previously described[16,45].

In this cohort and London as a whole infections peaked for the first pandemic wave of infections during the first week of lockdown (March 23rd 2020)[46], and we observed approximately synchronous exposure coincident with recruitment, we therefore used this as the benchmark for assessing exposure generated immunity. Across the main study cohort, 48 participants had positive RT-PCR results with 157 (21.5%) seropositive participants. 79% of positive PCR tests were within the first 2 weeks of follow-up and no HCW tested PCR+ after week 5 of follow-up (Fig. 1b)[14,46], with seroconversion within the first 3 weeks of follow-up for most[28]. Infections were asymptomatic or mild with only two hospital admissions (none requiring intensive care admission). The cross-sectional case controlled sub-study (n=129) collected samples at 16-18 weeks after the first UK lockdown (Fig. 1a). Power calculations were performed prior to week 16 sub-study sampling to determine the sample size needed to test the hypothesis that HCW with pre-existing T-cell responses are enriched in exposed seronegative group at a range of incidence of infection, assuming 50% of the total cohort had pre-existing T-cell responses. Sample sizes of 18-64 per group were estimated. An age, sex and ethnicity matched nested sub-study was designed within the larger (n=731) parent study and 129 attended for 16-week sampling including high volume PBMC isolation.

Laboratory-confirmed infection was determined by weekly nasopharyngeal RNA stabilizing swabs and reverse transcriptase polymerase chain reaction (RT-PCR; Roche cobas SARS-CoV-2 test, Envelope [E] gene) and antibody assay positivity (Spike protein 1 IgG Ab assay, EUROIMMUN) and anti-nucleocapsid total antibody assay (ROCHE) described in detail below. The seronegative health care worker group were matched for demographics and exposure to the laboratory-confirmed infected group and was defined by negativity by these 3 tests at all 16 time points as well as negative for neutralising antibodies at week 16 and at selected prior time points as indicated.

The cohort of medical students and laboratory staff was approved by UCL Ethics (Project ID Number:13545/001) and pre-pandemic healthy donor samples were collected and cryopreserved before August 2019 under ethics numbers 11/LO/0421. All subjects gave written informed consent and the study conformed to the principles of the Helsinki Declaration.

Isolation of PBMC and Serum

Peripheral blood mononuclear cells (PBMC) were isolated from heparinized blood samples using Pancoll (Pan Biotech) or Histopaque®-1077 Hybri-MaxTM (Sigma-Aldrich) density gradient centrifugation in SepMate tubes (StemCell) according to the manufacturer's specifications. Isolated PBMC were cryopreserved in fetal calf serum (FCS) containing 10% DMSO and stored in liquid nitrogen.

Whole blood samples were collected in SST vacutainers (VACUETTE) with inert polymer gel for serum separation and clot activator coating. After centrifugation at 1000 X g for 10 min at room temperature (RT), serum layer was aliquoted and stored at -80 °C. All T-cell assays reported here were performed on cryopreserved PBMC.

Weekly SARS-CoV-2 S1 and NP Serology

Weekly Euroimmun anti-SARS-CoV-2 enzyme-linked immunosorbent assay (ELISA; anti-SARS-CoV-2 S1 antigen IgG and the Roche Elecsys anti-SARS-CoV-2 electrochemiluminescence immunoassay (ECLIA; anti-SARS-CoV-2 nucleoprotein IgG/IgM) commercial assays were performed by Public Health England as previously described[16]. S1 ELISA: A ratio of ≥ 1.1 was deemed positive. A ratio of 11 was taken to be the upper threshold as the assay saturates beyond this point. NP ECLIA: Anti-NP results are expressed as a cut-off index (COI) value based on the electrochemiluminescence signal of a 2-point calibration, with results COI ≥1.0 classified as positive.

Neutralization assays – Pseudotype and authentic virus

SARS-CoV-2 pseudotype neutralisation assays were conducted using pseudotyped lentiviral particles as previously described[16]. Briefly, serum was heat-inactivated at 56 °C for 30 mins. Serum dilutions in DMEM were performed in duplicate with a starting dilution of 1 in 20 and 7 consecutive 2-fold dilutions to a final dilution of 1/2,560 in a total volume of 100 µl. 1×10^5 RLU of SARS-CoV-2 pseudotyped lentiviral particles were added to each well (serum dilutions and controls) and incubated at 37 °C for 1 hr. 4×10^4 Huh7 cells suspended in 100 µl complete media were added per well and incubated for 72 hr at 37 °C and 5% CO_2. Firefly luciferase activity (luminescence) was measured using Steady-Glo® Luciferase Assay System (Promega) and a CLARIOStar Plate Reader (BMG Labtech). The curves of relative infection rates (in %) versus the serum dilutions (log10 values) against a negative control of pooled sera collected prior to 2016 (Sigma) and a positive neutraliser were plotted using Prism 9 (GraphPad). A non-linear regression method was used to determine the dilution fold that neutralised 50% (IC50).

Authentic SARS-CoV-2 microneutralization assays were carried out as previously described[47]. Briefly, a mixture of serum dilutions in DMEM (1 in 20 and 11 consecutive 2-fold dilutions to a final dilution of 1/40,960) and 3×10^4 FFU of SARS-CoV-2 virus (Wuhan Hu-1) were incubated at 37 °C for 1 hr. After initial incubation, pre-seeded Vero E6 cells were infected with the serum-virus samples and incubated (37 °C and 5% CO_2) for 72 hr. Cells were then fixed with 100 µl 3.7% (vol/vol) formaldehyde for 1 hr. Cells were washed with PBS and stained with 0.1% (wt/vol) crystal violet solution for 10 minutes. After removal of excess crystal violet and air drying, the crystal violet stain was re-solubilized with 100 µl 1% (wt/vol) sodium dodecyl sulfate solution. Absorbance readings were taken at 570 nm using a CLARIOStar Plate Reader (BMG Labtech). Absorbance readings for each well were standardised against technical positive (virus control) and negative (cells only) controls on each plate to determine a percentage neutralisation value. A non-linear regression (curve fit) method was used to determine the dilution fold that neutralised 50% (IC50) using Prism 9 (GraphPad). SARS-CoV-2 is classified as a hazard group 3 pathogen and therefore all authentic SARS-CoV-2 propagation and microneutralization assays were performed in a containment level 3 facility.

Spike ELISA

Seropositivity against SARS-CoV-2 spike was determined for medical student and laboratory staff cohort between July 2020 and Jan 2021 (Extended Data Table 5) by enzyme-linked immunosorbent assay, as validated and described previously[40,48,49]. Briefly, 9 columns of 96-half-well MaxiSorp plates (Thermo Fisher Scientific) were coated overnight at 4 °C with purified S1 protein in PBS (3 µg/ml per well in 25 µl), the remaining 3 columns were coated with goat anti-human F(ab)'2 (1:1,000) to generate in internal standard curve. The next day, plates were washed with PBS-T (0.05% Tween in PBS) and blocked for 1 hr at RT with assay buffer (5% milk powder PBS-T). Sera were diluted in blocking buffer (1:50). 25 µl of serum was then added to S1 coated wells in duplicate and incubated for 2 hr at RT. Serial dilutions of known concentrations of IgG were added to the F(ab)'2 IgG-coated wells in triplicate (Sigma Aldrich). Following incubation for 2 hr at RT, plates were washed with PBS-T and 25 µl alkaline phosphatase-conjugated goat anti-human IgG (Jackson ImmunoResearch) at a 1:1000 dilution in assay buffer added to each well and incubated for 1 hr RT. Plates were then washed with PBS-T, and 25 µl of alkaline phosphatase substrate (Sigma Aldrich) added. ODs were measured using a MultiskanFC (Thermofisher Scientific) plate reader at 405 nm and S1-specific IgG

titers interpolated from the IgG standard curve using 4PL regression curve-fitting on GraphPad Prism 8.

HCoV spike Meso scale discovery immunoassay (MSD)

A multiplexed MSD immunoassay to measure anti-HCoV spike IgG antibodies was performed as previously described[50]. Plates were coated with 200-400 µg/ml spike protein (trimers in pre-fusion form) from the endemic human coronaviruses HKU1, OC43, 229E and NL63. Antibody concentration is presented in arbitrary units (AU) interpolated from the ECL signal of the internal standard sample using a 4-parameter logistic curve fit. Serum samples taken at wk8, the peak time point for Spike S1 IgG after PCR+ SARS-CoV-2 infection, were assayed for HCoV antibodies.

SARS-CoV-2 spike-specific memory B-cell staining

Multiparameter flow cytometry was used for *ex vivo* identification of spike-specific memory B cells staining as previously described[29]. Biotinylated tetrameric spike (1 µg) was fluorochrome linked by incubating with streptavidin conjugated APC (Prozyme) and PE (Prozyme) for 30 mins in the dark on ice. PBMC were thawed and incubated with Live/Dead fixable dead cell stain (UV, ThermoFisher Scientific) and saturating concentrations of phenotyping mAbs diluted in 50% 1 x PBS 50% Brilliant Violet Buffer (BD Biosciences): CD3 Bv510 (Biolegend, clone OKT3, 1:200), CD11c FITC (BD Biosciences, clone B-ly6, 1:100), CD14 Bv510 (Biolegend, clone M5E2, 1:200), CD19 Bv786 (BD Bioscience, clone HIB19, 1:50), CD20 AlexFluor700 (BD Biosciences 2H7, 1:100), CD21 Bv711 (BD Biosciences, clone B-ly4, 1:100), CD27 BUV395 (BD Biosciences, clone L128, 1:100), CD38 Pe-CF594 (BD Biosciences, clone HIT2, 1:200), IgD Pe-Cy7 (BD Biosciences, clone IA6-2, 1:100). For identification of SARS-CoV-2 antigen specific B cells 1 µg per 500 µl of stain each of tetrameric Spike-APC and Spike-PE were added to cells. Cells were incubated in the staining solution for 30 mins RT, washed with PBS, and subsequently fixed with FoxP3 Buffer Set (BD Biosciences) according to the manufacturer's instructions. All samples were acquired on a BD Fortessa-X20 flow cytometer. Data were analysed by FlowJo version 10.7 (TreeStar). Example gating and positivity cut-off have been previously reported[29]. The magnitude of the SARS-CoV-2 spike-specific memory B cell population is expressed as a percentage of memory B cells (gated as: lymphocytes, singlets, Live, CD3-CD14-CD19+, CD20+, excluding: $CD38^{hi}$, IgD+ and CD27+CD21-) binding both PE- and APC-labelled spike.

SARS-CoV-2 peptides

Full lists of the peptides contained in pools of overlapping peptides covering structural[16] and RTC proteins[8] have been previously described (15mer peptides overlapping by 10 amino acids, GL Biochem Shanghai Ltd, >80% purity). Overlapping peptides of NSP12 are listed in Supplementary Table 3. For IFNγ-ELISpot assays SARS-CoV sequence peptides were used (96.5% sequence homology with Wuhan SARS-CoV-2 consensus sequence, 34/931 amino acids differ, Supplementary Table 3). For epitope mapping SARS-CoV-2 sequence peptides were used for NSP12-2 and NSP12-5 (GL Biochem Shanghai Ltd, >80% purity).

To limit competition for *in vitro* for peptide presentation we limit stimulations to a maximum of 55 peptides and have, therefore, divided large proteins such as NP into subpools: NP (NP1, NP2, 41 peptides each), M (43 peptides), ORF3a (53 peptides), NSP7 (15), NSP12 (36-37 per pool NSP12-1 to NSP12-5) and NSP13 (39-40 peptides per pool NSP13-1 to NSP13-3). In addition 15mer peptides covering the predicted SARS-CoV-2 spike epitopes[8] to give a total of 55 peptides in this pool (Spike). Optimal 9mer peptides for CD8+ epitopes were custom synthesised by ThinkPeptides (UK) >70% purity (Supplementary Table 3).

IFNγ-ELISpot Assay

IFNγ-ELISpot Assay was performed as previously described on cryopreserved PBMC[8,16,51]. Unless otherwise stated, culture medium for human PBMC (R10) was sterile 0.22 µM filtered RPMI medium (Thermo Fisher Scientific) supplemented with 10% by volume heat inactivated (1 hr, 64 °C) FCS (Hyclone) and 1% by volume 100 x penicillin and streptomycin solution (GibcoBRL).

ELISpot plates (Merck-Millipore, MSIP4510) were coated with human anti-IFNγ Ab (1-D1K, Mabtech; 10 µg/ml) in PBS overnight at 4 °C. Plates were washed 6x with sterile PBS and were blocked with R10 for 2 hr at 37 °C with 5% CO_2. PBMC were thawed and rested in R10 for 3 hr at 37 °C with 5% CO_2 before being counted to ensure only viable cells were included. 400,000 PBMC/well were seeded in R10/well and were stimulated for 16-20 hr with SARS-CoV-2 peptide pools (2 µg/ml per peptide) at 37 °C in a humidified atmosphere with 5% CO_2. Where insufficient T-cells were available NSP12 pools 1,2 and 3 and NSP13 pools 1,2,3 were combined into a single well. For baseline measurements NSP12 pools 1-5 were stimulated in a single well and where insufficient T-cells were available a single DMSO well was included. HCW who did not have a full complement of stimulations were excluded from analysis of total magnitude of breadth of response, hence slightly lower n numbers. Internal plate controls were R10 alone (without T-cells) and two DMSO wells (negative controls), concanavalin A (ConA, positive control; Sigma-Aldrich) and FEC (HLA I-restricted peptides from influenza, Epstein-Barr virus, and CMV; 1 µg/ml per peptide). ELISpot plates were developed with human biotinylated IFNγ detection antibody (7-B6-1, Mabtech; 1µg/ml) for 3 hr at RT, followed by incubation with goat anti-biotin alkaline phosphatase (Vector Laboratories; 1:1000) for 2 hr RT, both diluted in PBS with 0.5% BSA by volume (Sigma-Aldrich), and finally with 50 µl/well of sterile filtered BCIP/NBT Phosphatase Substrate (ThermoFisher) for 7 min RT. Plates were washed in ddH_20 and left to dry overnight before being read on an AID classic ELISpot plate reader (Autoimmun Diagnostika GMBH, Germany).

The average of two DMSO wells was subtracted from all peptide-stimulated wells for a given PBMC sample and any response that was lower in magnitude than 2 standard deviations of these sample specific DMSO control wells was not considered a peptide specific response (given value 0). Results were expressed as IFNγ spot forming cells (SFC) per 10^6 PBMC after background subtraction. The geometric mean of all DMSO wells was 9.571 SFC per 10^6 PBMC (3.8 spots). We excluded the results if negative control wells had >95 SFC/10^6 PBMC or positive control wells (ConA) were negative. T-cell responses to SARS-CoV-2 did not correlate with background spots in DMSO wells (e.g. SN-HCW group, Spearman r = -0.068 p = 0.6141).

Antigen-specific T-cell proliferation assay and epitope mapping

Frozen PBMC were thawed and washed twice with sterile PBS. PBMC were resuspended in 1 mL R10 culture media (2-10 x 10^6 PBMC) and 0.5 µL of 5 mM stock CellTrace violet (CTV; Thermo Fisher Scientific) was added per sample with mixing. PBMC were stained in the dark for 10 mins at 37 °C in a humidified atmosphere with 5% CO_2. 10-times volume of cold R10 was added to stop the staining reaction, and cells were incubated for 5 mins on ice. Cells were washed in PBS and incubated for 5 mins at 37 °C before being transferred to a new tube and were washed again in R10. CTV stained PBMC were plated in 96-well plates (2-4 x 10^5 PBMC in 200 µL R10) and stimulated with peptide pools (2 µg/ml per peptide) for 10 days in R10 supplemented with 0.5 µg/ml soluble anti-CD28 (Thermo Fisher scientific) and 20 U/ml recombinant human IL2 (Peprotech). CTV-stained and unstained PBMC were run to confirm efficiency of staining. 100 µL media was added on day 1, and 100 µL media removed and replaced with R10 supplemented with anti-CD28 and IL2 as above on days 3 and 6. On day 9 PBMC were re-stimulated with peptide pools (2 µg/ml per peptide) and brefeldin A (10 µg/ml; Sigma-Aldrich). After 16-18 hr re-stimulation PBMC were harvested, washed in PBS, and stained for fixable live/dead (Near infrared, Thermo Fisher Scientific, 1:1000), washed in PBS, before being fixed in Fix/perm buffer (TF staining buffer kit, eBioscience) for 20 mins RT. Cells were washed in PBS and incubated in perm buffer (TF staining buffer kit, diluted 1:10 in ddH_2O) for 20 mins RT, washed in PBS and resuspended in perm buffer with saturating concentrations of

anti-human antibodies for intracellular staining: IL-2 PerCp-eFluor710 (Invitrogen, clone MQ1-17H12, 1:50), TNFα FITC (BD Bioscience, clone MAb11, 1:100), CD8α BV785 (Biolegend, clone RPA-T8, 1:200), IFNγ BV605 (BD Biosciences, clone B27, 1:100), IFNγ APC (Biolegend, clone 4S.B3, 1:50), CD3 BUV805 (BD Biosciences, clone UCHT1, 1:200), CD4 BUV395 (BD Biosciences, clone SK3, 1:200), CD154 (CD40L) Pe-Cy7 (Biolegend, clone 24-31, 1:50), MIP-1-β PE (BD Biosciences, clone D21-1351, 1:100). Cells were washed twice in PBS and analysed on a BD LSRII flow cytometer. Cytometer voltages were consistent across batches. FMOs and unstimulated samples were used to determine gates applied across samples. Data were analysed by FlowJo version 10.7 (TreeStar).

Optimisation experiments showed use of rhIL2 increases non-peptide specific proliferation of T-cells but is essential for optimal expansion of proliferating cytokine producing peptide-specific T-cells. CTV dilution and staining with anti-human-IFNγ antibodies was used to identify antigen-specific T-cells. An unstimulated control well (equivalent DMSO to peptide wells added) was included for each PBMC sample and the percentage of CTV^{lo} IFNγ+ CD4+ or CD8+ proliferating in unstimulated wells was subtracted as background cytokine release from all peptide stimulated wells. The T-cell proliferation assay above was used to expand SARS-CoV-2-specific T-cells and a 2-dimension matrix (Supplementary Table 2) was employed so that each 15mer peptide was represented in 2 pools aiding the identification of individuals immunogenic 15mer peptides. T-cell responses were then confirmed by repeated expansion with individual 15mers.

Polyfunctionality, defined as the number of cytokines co-produced by T-cells after 10-day expansion, was assessed using SPICE (version 6.0) and pestle (version 2.0), available at https://niaid.github.io/spice/[52]. Responses <0.1% of CD4+ or CD8+ T-cells were excluded. Boolean gating was used to identify the percentage of T-cells making the 31 possible combinations of the following cytokines: IFNγ, TNF, IL-2, CD154, MIP-1-β. Pestle was used to background subtract the percentage of cytokine producing cells from unstimulated wells ran in parallel and to format data for visualisation in SPICE. The proportion of T-cells making a specific number of cytokines in combination is presented as pie graphs (base mean) and pie arcs represent the proportion making a given cytokine. The RTC-specific T-cell polyfunctionality was calculated as an average over T-cell responses to NSP7, NSP12 and NSP13 and the structural-specific T-cell polyfunctionality is an average of responses to Spike, ORF3a, M and NP (Extended Data Fig. 3d).

MHC class I pentamer staining

HLA-A*02-restricted pentamers (Proimmune) of the following specificities were used: SARS-CoV-2 $NSP7_{27\text{-}35}$ (KLWAQCVQL) or HCoV HKU1 $NSP7_{27\text{-}35}$ (KLWQYCSVL; *ex vivo* stains only). For post-expansion staining: antigen-specific T-cells were expanded with cognate 9mer peptide of SARS-CoV-2 or HCoV HKUW sequence for 8-10 days as above (2 µg/ml per peptide) in R10 supplemented with 0.5 µg/ml soluble anti-CD28 and 20 U/ml recombinant human IL2; media added on days 1, 3 and 6 prior to pentamer staining. For *ex vivo* staining: PBMC were thawed, washed twice in PBS. Pentamers were centrifuged at 13,000 rpm for 10mins prior to use. 0.5-2 x 10^6 PBMC were stained with 1µl pentamers at RT for 20mins in 50 µl PBS in a 96-well plate. PBMC were further stained with Blue fixable Live/dead (Invitrogen, 1:1000) for 20mins at 4 °C, and surface stained with a mixture of saturating concentrations of mAbs for 30mins at 4 °C: CD3 BUV805 (BD Biosciences, clone UCHT1, 1:200), CD4 BUV395 (BD Biosciences, clone SK3, 1:200), CD56 Pe-Cy7 (BD Biosciences, NCAM16.2, 1:100), CD8α Alexa700 (Biolegend, RPA-78, 1:200), post-expansion CD19 Bv786 (BD Biosciences, HIB19, 1:100). PBMC were fixed with 1% paraformaldehyde and flow cytometry was performed as above using a BD LSRII flow cytometer. Data were analysed by FlowJo version 10.7 (TreeStar). During analysis, stringent gating criteria were applied (Gating strategy in Extended Data Fig. 6c) with doublet, dead cell, CD19+ B cell (post-expansion) and CD56+ NK/NKT exclusion to minimize nonspecific binding contamination. HLA-mismatched PBMC (non-HLA-A*02) and fluorescence minus one controls for pentamers were stained in parallel to assess non-specific binding (Extended Data Fig. 6c).

Coronaviridae family sequence homology analyses

The sequence homology of SARS-CoV-2-derived peptides to HCoV sequences was computed as previously described[32]. Briefly, the SARS-CoV-2 proteome (NC_045512.2) was decomposed into 15mer peptide sequences overlapping by 14 amino acids. A protein BLAST search of each 15mer peptide was then performed against a custom sequence database comprising 2531 *Coronaviridae* sequences[32]. Homology values of each SARS-CoV-2-derived peptide to viral accessions with '229E', 'OC43', 'NL63', or 'HKU1' included in the species name and that were isolated from human hosts were retained (Supplementary Table 1). Additionally, to determine if the conservation of 15mer peptides differed between the SARS-CoV-2 proteins, the average homology of peptides within each protein was computed. A permutation test was conducted to test if the difference in average homology between the two proteins, Δh, was statistically significant. Briefly, the protein membership of each 15mer peptide was permuted (1000 iterations). The Δh of two proteins were then calculated at each iteration, resulting in a final null distribution of Δh values. *P*-values were computed as the number of permutations that yielded a Δh at least as extreme as the observed Δh of the two proteins. Custom scripts used to perform the homology searches, heatmap visualisation and permutation testing are hosted on GitHub: https://github.com/cednotsed/tcell_cross_reactivity_covid.git.

For sequence alignments of immunogenic 15mers or at described MHC class I-restricted epitopes reference protein sequences for ORF1ab (accession numbers: QHD43415.1, NP_828849.2, YP_009047202.1, YP_009555238.1, YP_173236.1, YP_003766.2 and NP_073549.1) were downloaded from the NCBI database (https://www.ncbi.nlm.nih.gov/protein/) as previously described[8]. Sequences were aligned using the MUSCLE algorithm with default parameters and percentage identity was calculated in Geneious Prime 2020.1.2, www.geneious.com. Alignment figures were made in Snapgene 5.1 (GSL Biotech).

SARS-CoV-2 species genome diversity analyses

For genome diversity analysis a complete masked alignment was downloaded from the GISAID[53,54] EpiCoV database on 26/7/2021 together with a GISAID Audacity phylogeny comprising 611,893 accessions (Full list and metadata available at:

https://figshare.com/s/049d53f789a8b111b87e). The alignment was subsampled to include 800 of each defined NextStrain phylogenetic clade, as provided by GISAID metadata. For clades containing less than 800 accessions all representatives of that clade were included resulting in a comprehensive sampling over the global phylogeny of 13,785 accessions encompassing the genomic diversity of SARS-CoV-2 to date (Extended Data Fig. 5a). Diversity along the genome was assessed using two metrics of diversity: the number of recurrent mutational emergences (homoplasies) at any position and Nei's genetic diversity index[55]. Homoplasy counts per locus were computed via application of the HomoplasyFinder screening pipeline[56] against a maximum likelihood phylogeny constructed over the 13,785 genome alignment. Nei's genetic diversity index was computed as $H = 1 - \sum_{i=1}^{I} p_i^2$, where I is the count of distinct alleles at a position, and $p_i = (i = 1, \ldots, I)$ is the frequency of allele i in the studied alignment. The average homoplasy count per locus per gene region and average Nei's genetic diversity per gene region were computed by normalising the per locus values by gene length for all ORF and NSP according to the reference annotations of GISAID reference genome EPI_ISL_402124. Significant differences between all pairwise combinations of ORF/NSP was assessed using the Wilcoxon rank sum test implemented in *compare_means()* in the R package ggpubr v0.4.0 (Extended Data Table 3).

IFI27 qPCR

Total RNA from Tempus blood was extracted using the Tempus Spin RNA isolation kit (Applied Biosystems, 4380204). cDNA was obtained

using the High-Capacity cDNA Reverse Transcription Kit (Applied Biosystems). Quantitative PCR was performed using the TaqMan™ Fast Advanced Master Mix (Applied Biosystems) on ABI StepOnePlus Real-Time PCR machine (Applied Biosystems). The following cycling conditions were used: 95 °C for 2 mins, followed by 40 cycles of 95 °C for 3 s and 60 °C for 30 s. *IFI27* and *GAPDH* were amplified using the TaqMan Gene Expression Assay probes-Hs01086373_g1 (IFI27) and Hs02786624_g1 (GAPDH) respectively. *GAPDH* was used as a housekeeping gene control. Unexposed pre-pandemic control HCW cohort for qPCR described previously[57]

Correlogram plot

A pairwise correlation matrix between variables was calculated and visualised as a correlogram using corrplot (https://github.com/taiyun/corrplot) in R version 3.5.3 with R studio version 1.0.153. Spearman's rank correlation coefficient r is indicated by the size and colour of the circles. Only correlations with a $p < 0.05$ are shown. Variables are ordered by hierarchical clustering.

Statistics and reproducibility

Data was assumed to have a non-Gaussian distribution and nonparametric tests were used throughout. For single paired and unpaired comparisons Wilcoxon matched-pairs signed rank test and a Mann-Whitney U test were used. For multiple unpaired comparisons Kruskal-Wallis one-way ANOVA with Dunn's correction was used. For correlations, Spearman's r test was used. A p value <0.05 was considered significant. Prism v. 7.0e and 8.0 for Mac was used for analysis. Details are provided in figure legends.

Data reporting

Power calculations were used to estimate the sample size needed for week 16 sub-study (see above). No statistical methods were used to predetermine sample size. For all assays samples from each cohort were run in parallel to reduce the impact of inter-batch technical variation. IFNγ-ELISpot assays were performed on HCW cohorts prior to unblinding of group (laboratory-confirmed infection or SN-HCW). Other experiments were not randomized and the investigators were not blinded to allocation during experiments and outcome assessment.

Reporting summary

Further information on research design is available in the Nature Research Reporting Summary linked to this paper.

Data availability

All data analysed during this study are included in this published article (and its supplementary information files). Custom scripts used to perform the homology searches, heatmap visualisation and permutation testing are hosted on GitHub (https://github.com/cednotsed/tcell_cross_reactivity_covid.git). Genomic data analysed was obtained from the publicly available NCBI Virus database and, following registration, from the GISAID EpiCoV repository. The datasets generated during and/or analysed during the current study are available from the corresponding author on reasonable request. Correspondence and requests for materials should be addressed to MKM or LS. Source data are provided with this paper.

45. Augusto, J. B. et al. Healthcare Workers Bioresource: Study outline and baseline characteristics of a prospective healthcare worker cohort to study immune protection and pathogenesis in COVID-19. *Wellcome Open Res.* **5**, 179 (2020).
46. Treibel, T. A. et al. COVID-19: PCR screening of asymptomatic health-care workers at London hospital. *Lancet* **395**, 1608–1610 (2020).
47. Reynolds, C. J. et al. Prior SARS-CoV-2 infection rescues B and T cell responses to variants after first vaccine dose. *Science* **5**, 1–11 (2021).
48. O'Nions, J. et al. SARS-CoV-2 antibody responses in patients with acute leukaemia. *Leukemia* **35**, 289–292 (2021).
49. Muir, L. et al. Neutralizing Antibody Responses After SARS-CoV-2 Infection in End-Stage Kidney Disease and Protection Against Reinfection. *Kidney Int. Reports* (2021) https://doi.org/10.1016/j.ekir.2021.03.902.
50. Johnson, M. et al. Evaluation of a novel multiplexed assay for determining IgG levels and functional activity to SARS-CoV-2. *J. Clin. Virol.* **130**, 104572 (2020).
51. Capone, S. et al. Optimising T cell (re)boosting strategies for adenoviral and modified vaccinia Ankara vaccine regimens in humans. *npj Vaccines* **5**, 1–14 (2020).
52. Roederer, M., Nozzi, J. L. & Nason, M. C. SPICE: Exploration and analysis of post-cytometric complex multivariate datasets. *Cytom. Part A* **79 A**, 167–174 (2011).
53. Shu, Y. & McCauley, J. GISAID: Global initiative on sharing all influenza data – from vision to reality. *Eurosurveillance* **22**, 30494 (2017).
54. Elbe, S. & Buckland-Merrett, G. Data, disease and diplomacy: GISAID's innovative contribution to global health. *Glob. Challenges* **1**, 33–46 (2017).
55. Nei, M. Analysis of gene diversity in subdivided populations. *Proc. Natl. Acad. Sci. U. S. A.* **70**, 3321–3323 (1973).
56. Crispell, J., Balaz, D. & Gordon, S. V. HomoplasyFinder: a simple tool to identify homoplasies on a phylogeny. *Microb. genomics* **5**, (2019).
57. Pollara, G. et al. Exaggerated IL-17A activity in human in vivo recall responses discriminates active tuberculosis from latent infection and cured disease. *Sci. Transl. Med.* **13**, 7673 (2021).

Acknowledgements We are extremely grateful to all patients and control volunteers who participated in this study and to all clinical staff who helped with recruitment and sample collection. We are grateful to Jamie Evans at the Rayne Building FACS facility for assistance with flow cytometry assays. We gratefully acknowledge all contributing and submitting laboratories around the globe who have openly shared large numbers of UK SARS-CoV-2 assemblies. A full list of acknowledgements providing submitting and originating laboratories is provided at: https://figshare.com/s/049d53f789a8b111b87e. The COVIDsortium is supported by funding donated by individuals, charitable Trusts, and corporations including Goldman Sachs, Citadel and Citadel Securities, The Guy Foundation, GW Pharmaceuticals, Kusuma Trust, and Jagclif Charitable Trust, and enabled by Barts Charity with support from UCLH Charity. Wider support is acknowledged on the COVIDsortium website. Institutional support from Barts Health NHS Trust and Royal Free NHS Foundation Trust facilitated study processes, in partnership with University College London and Queen Mary University London. This study was funded by UKRI/NIHR UK-CIC (supporting LS and MKM). MKM is also supported by Wellcome Trust Investigator Award (214191/Z/18/Z) and CRUK Immunology grant (26603) and LS by a Medical Research Foundation fellowship (044-0001). MN is supported by the Wellcome Trust (207511/Z/17/Z) and by NIHR Biomedical Research Funding to UCL and UCLH. AB is supported by Grant support a Special NUHS COVID-19 Seed Grant Call, Project NUHSRO/2020/052/RO5+5/NUHS-COVID/6 (WBS R-571-000-077-733). JCM, CM and TAT are directly and indirectly supported by the University College London Hospitals (UCLH) and Barts NIHR Biomedical Research Centres and through the British Heart Foundation (BHF) Accelerator Award (AA/18/6/34223). TAT is funded by a BHF Intermediate Research Fellowship (FS/19/35/34374). AMV, ÁM, CM and JCM were supported by the UKRI/MRC Covid-19 Rapid response grant COV0331. ÁM and CP are supported by Rosetrees Trust, The John Black Charitable Foundation, and Medical College of St Bartholomew's Hospital Trust and NIHR-MRC grant MR/V027883/1. RJB and DMA are supported by MRC (MR/S019553/1, MR/R02622X/1, MR/V036939/1, MR/W020610/1), NIHR Imperial Biomedical Research Centre (BRC): ITMAT, Cystic Fibrosis Trust SRC (2019SRC015), and Horizon 2020 Marie Skłodowska-Curie Innovative Training Network (ITN) European Training Network (No 860325). Funding for the HLA imputed data was provided by UKRI/MRC Covid-19 rapid response grant (Cov-0331 - MR/V027883/1). LEM is supported by a Medical Research Council Career Development Award (MR/R008698/1). LVD is supported by a UCL Excellence Fellowship. The funders had no role in study design data collection, data analysis, data interpretation, or writing of the report.

Author contributions MKM conceived the project and obtained funding. LS, MN, AB and MKM designed experiments. CM, TAT, JCM, MN, ÁM established the HCW cohort. LS, MOD, NMS, OEA, CP, JMG, SK, GAM, JR, JD, GJ, collected or processed HCW samples with COVIDsortium investigators. MKM, LS, MN, and ESW established medical student/laboratory staff and pre-pandemic cohorts (UK). LEM, MJ, DG and COVIDsortium investigators performed serology. MKM and LS designed T-cell experiments. LS, MOD, NMS, OEA, developed, performed and analysed the T-cell experiments. AB, NLB, ATT, CYLT performed T-cell assays and analysed data from pre-pandemic cohort (Singapore). AC performed and analysed blood transcriptomic experiments. AMV supervised HLA analysis. ÁM supervised nAb experiments. JMG and CP performed and analysed nAb experiments. CCST, LVD, FB performed viral sequence analysis. ESW, MPJ, GJ, RJB, CM, TAT, JCM, ÁM, MD, provided or processed essential clinical data. MJ and DG performed and analysed HCoV serology. LS, MOD, NMS, OEA, AC, CP, JMG, NLB, ATT, AJS, CCST, CYLT, AMV, BMC, DG, LVD, DMA, RJB, CM, TAT, LEM, FB, ÁM, MN, AB, and MKM analysed and interpreted the data. LS and MKM prepared the manuscript. All authors provided critical review of the manuscript.

Competing interests A.B. is a cofounder of Lion TCR, a biotechnology company that develops T-cell receptors for the treatment of virus-related diseases and cancers. RJB and DMA are members of the Global T-cell Expert Consortium and have consulted for Oxford Immunotec outside the submitted work. All other authors have no competing interests related to the study.

Additional information

Supplementary information The online version contains supplementary material available at https://doi.org/10.1038/s41586-021-04186-8.

Correspondence and requests for materials should be addressed to Leo Swadling or Mala K. Maini.

Peer review information *Nature* thanks Stanley Perlman and the other, anonymous, reviewer(s) for their contribution to the peer review of this work. Peer reviewer reports are available.

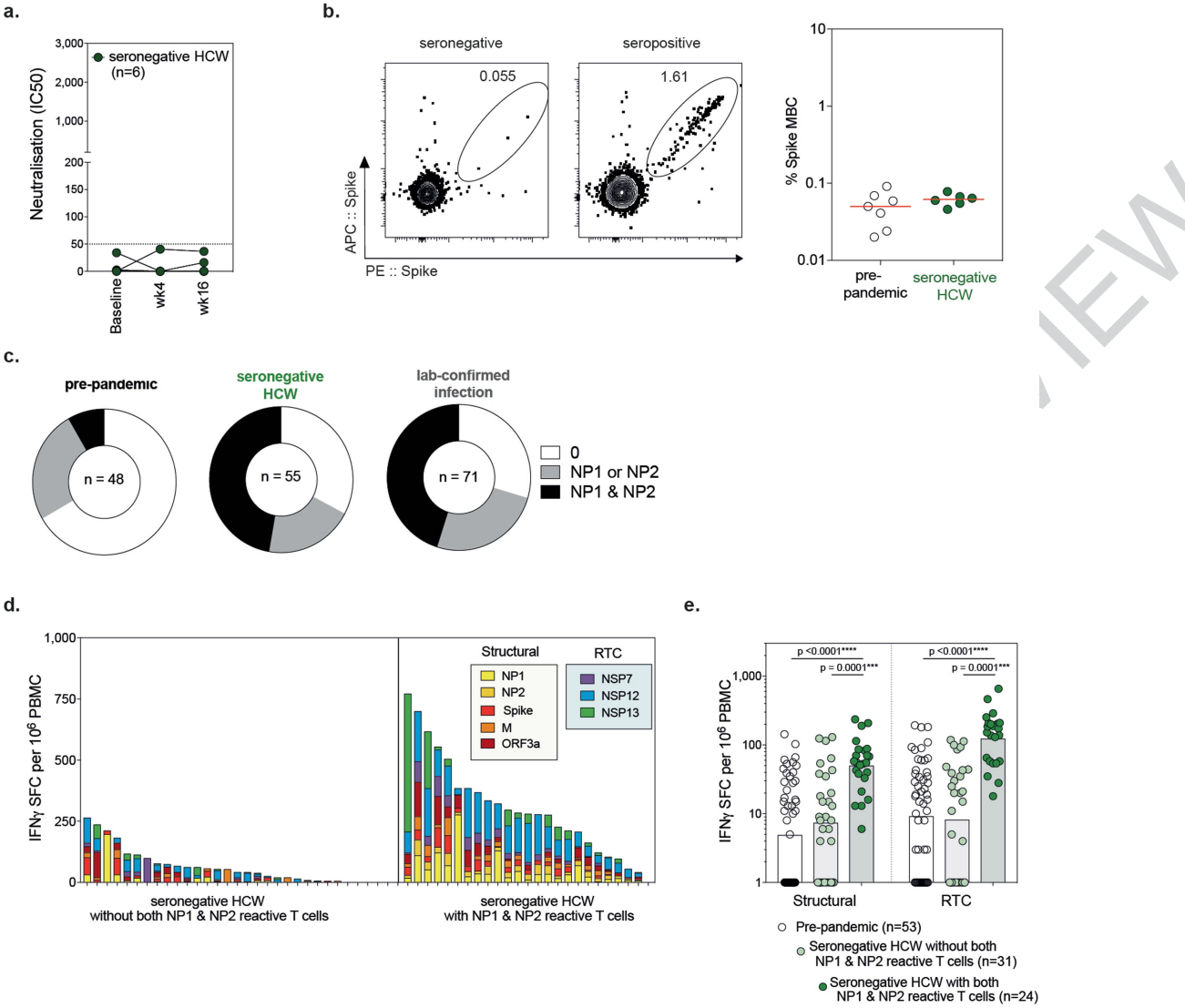

Extended Data Fig. 1 | SARS-CoV-2 immunity in seronegative HCW – authentic virus neutralisation and T-cell response in those with NP1+NP2 responses. a, authentic virus neutralisation (Wuhan Hu-1). **b**, Example plots of SARS-CoV-2 spike memory B cell (MBC) staining (gated on: lymphocytes/singlets/Live, CD3-CD14-CD19+/CD20+, excluding CD38^{hi}, IgD+ and CD21+CD27- fractions) and frequency of SARS-CoV-2 spike-specific MBC in pre-pandemic or SN-HCW (wk16; as a percentage of total MBC). Bars, median. **c**, Proportion of cohorts with T-cell responses to NP1 and/or NP2 subpools. **d**, Magnitude of T-cell response coloured by viral protein and **e**, summed response to RTC and structural regions in SN-HCW with T-cells reactive against both NP1 and NP2 and against one of or neither NP1 or NP2 pools at wk16. Kruskal-Wallis with Dunn's correction. Bars, geomean. **a-e**, COVIDsortium HCW cohort. NP, nucleoprotein; RTC, replication-transcription complex.

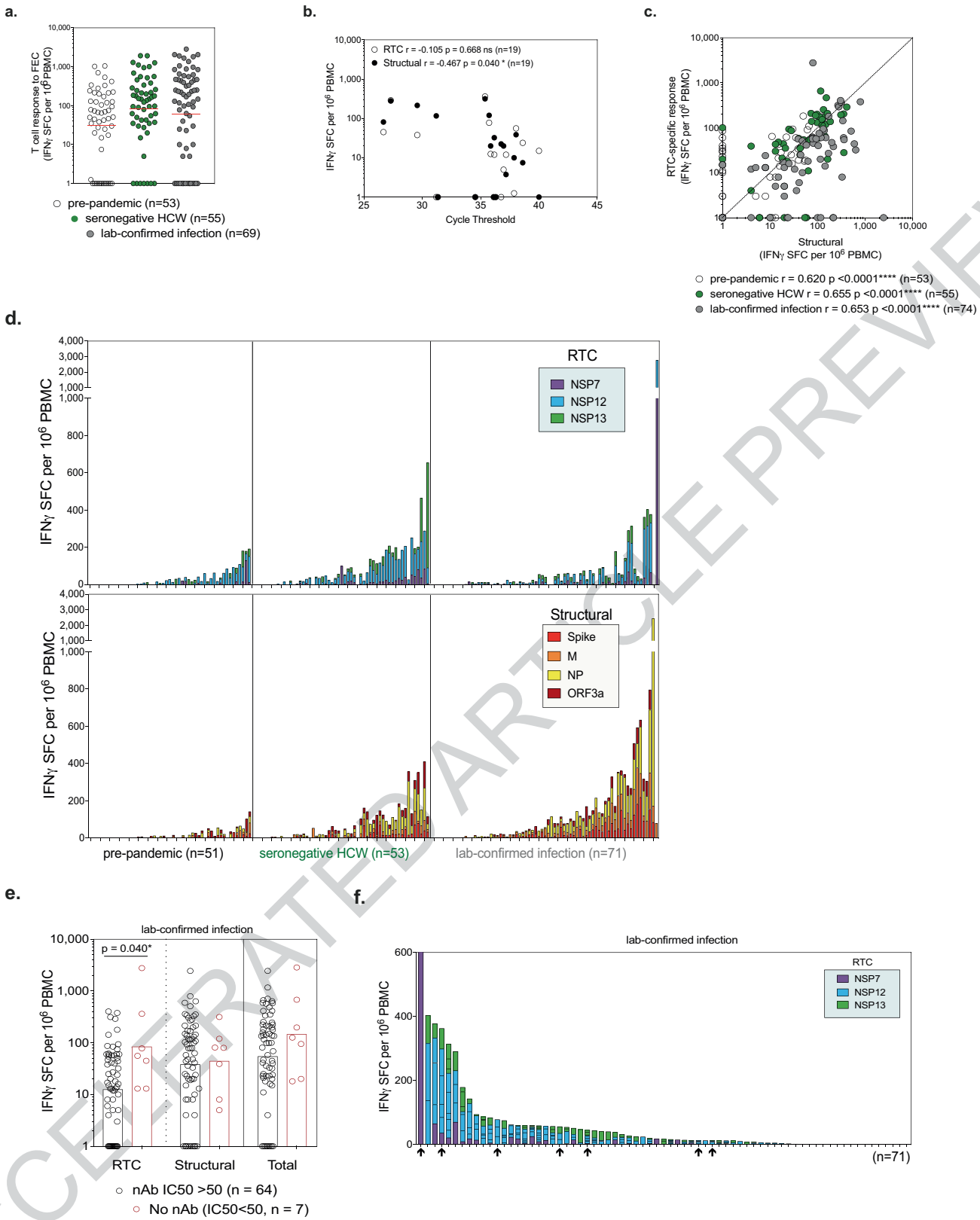

Extended Data Fig. 2 | T-cell responses to RTC and structural regions of SARS-CoV-2 by cohort. a, T-cell response to Flu, EBV and CMV (FEC) MHC class I restricted peptide pool. **b**, E gene RT-PCR cycle threshold value vs. magnitude of T-cell response to RTC or structural proteins in HCW with laboratory-confirmed infection. **c**, Magnitude of T-cell response to RTC vs. structural regions. **d**, Magnitude of T-cell response to RTC (top) and structural regions (bottom) coloured by specificity. **e**, Magnitude of T-cell response in laboratory-confirmed infection group in HCW with or without detectable nAb at wk16. **f**, T-cell response to RTC coloured by protein in laboratory-confirmed infection group ordered by magnitude. HCW lacking neutralising antibodies highlighted by arrows below. **a-f**, IFNγ-ELISpot wk16. **a**, Red lines, geomean. **e**, Bars, geomean. **b-c** Spearman r. **a,d** Kruskal-Wallis ANOVA with Dunn's correction. **a-f**, COVIDsortium HCW cohort.

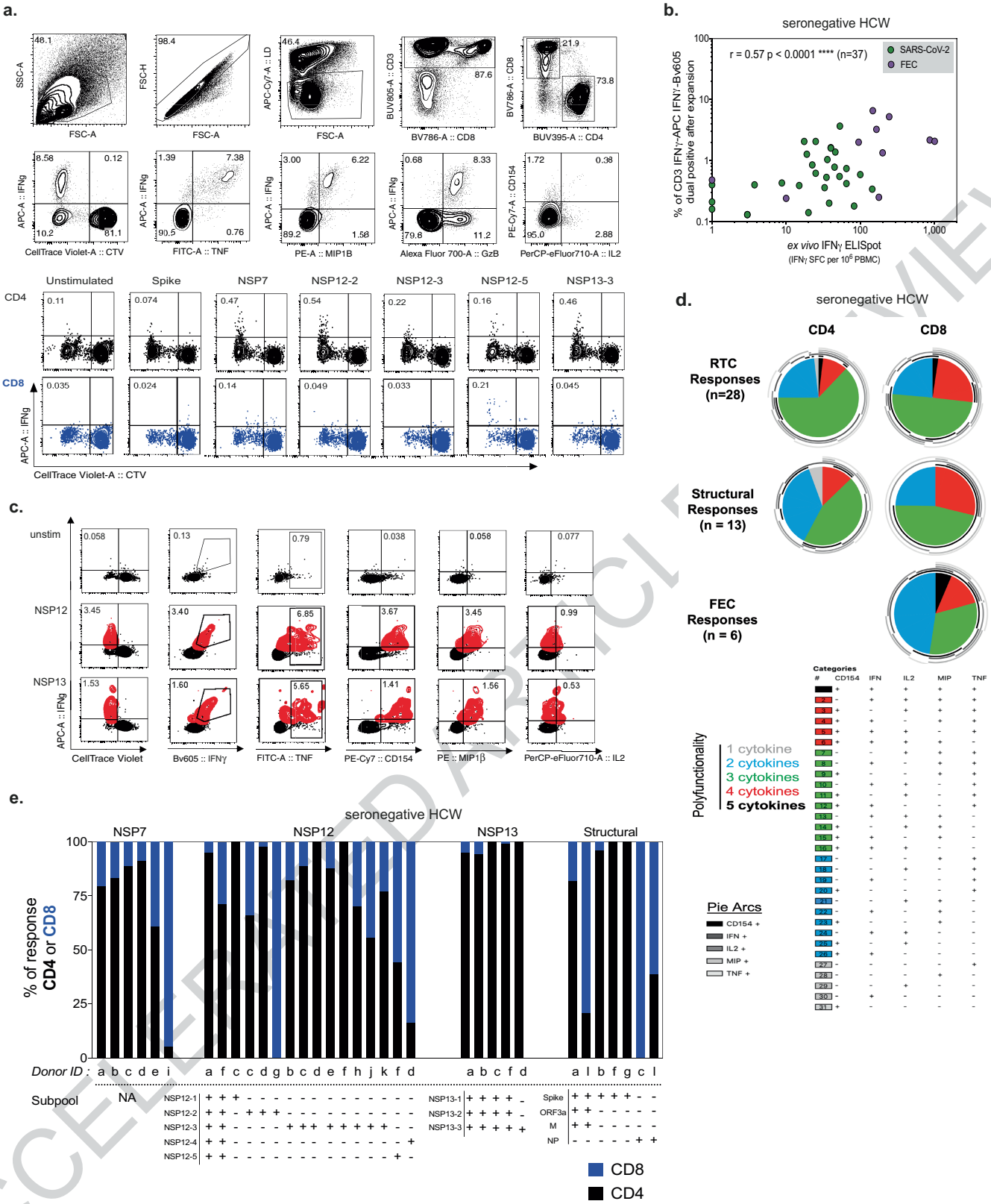

Extended Data Fig. 3 | See next page for caption.

Extended Data Fig. 3 | Functional and proliferative SARS-CoV-2 specific T-cells in seronegative HCW. a, (Upper) Example gating of CTV stained PBMC after 10-day peptide stimulation: Lymphocytes (SSC-A vs. FSC-A), single cells (FSC-H vs. FSC-A), Live cells (fixable live/dead-), CD3+, CD4+ or CD8+. Second row: Gated on CD8+ showing cytokine/intracellular protein combinations. Response to immunodominant MHC class I-restricted peptide pool against Flu, EBV, CMV (FEC) in SN-HCW. (Lower) example CTV and IFNγ staining in a SN-HCW (gated on CD4+ [black] or CD8+ [blue] T-cells, percentage $CTV^{lo}IFN\gamma^{+}$ shown). **b**, Correlation between the magnitude of T-cells responses to SARS-CoV-2 pools or FEC after 10-day *in vitro* expansion (% dual staining for two anti-human IFNγ mAb clones, responses <0.1% of CD3 post-expansion excluded) and *ex vivo* IFNγ-ELISpot in SN-HCW. Spearman r. **c**, Example plots of dual cytokine or activation marker staining of SARS-CoV-2-specific T-cells in an SN-HCW after 10-day expansion with peptide pools (proliferating T-cells become CTV^{lo} as they divide and dilute out marker). SARS-CoV-2-specific T-cells highlighted in red ($CD4+ CTV^{lo}IFN\gamma^{+}$). Percentage of CD4+ shown. **d**, polyfunctionality of CD4+ and CD8+ T-cells targeting the RTC or structural regions of SARS-CoV-2 or FEC peptide pool (proportion of cytokine producing T-cells that co-producing a given number of cytokines after 10-day peptide stimulation). Pie base, mean. Pie arcs show proportion of cells producing a given cytokine. **e**, Proportion of SARS-CoV-2-specific T-cells ($CTV^{lo}IFN\gamma+$) that are CD4+ or CD8+ after 10-day expansion (the protein specificity is listed above, donor ID (**a-l**, corresponding to raw data in Extended Data Table 2) and peptide subpools used for stimulation listed below). **a-e**, SN-HCW at wk16 COVIDsortium HCW cohort.

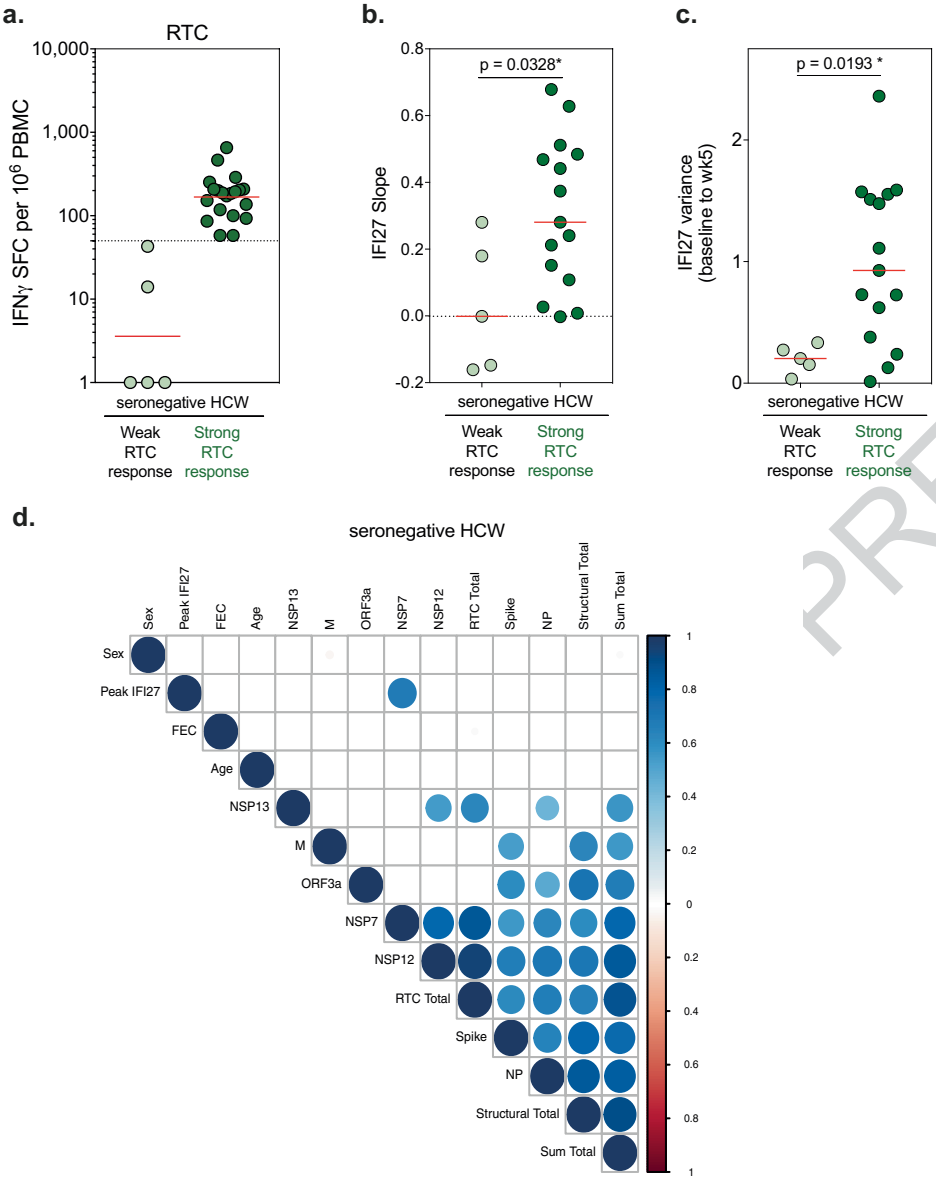

Extended Data Fig. 4 | Slope and variance of IFI27 signal in seronegative HCW. a, Subsetting SN-HCW group into those with weak (n=5, <50 SFC/10^6 PBMC) or strong (n=20, >50 SFC/10^6 PBMC) RTC-specific T-cell responses at wk16. **b**, Slope and **c**, variance of IFI27 signal (wk0-5) in SN-HCW with weak (n=5) or strong (n=15) RTC-specific T-cell responses at wk16. **d**, Correlation matrix of variables for SN-HCW (colour and size of dots represent spearman's r, only correlations p<0.05 shown; peak IFI27 signal from wk0-5, T-cell responses at wk16 to proteins, regions [RTC or structural], or total SARS-CoV-2 response). **b,c**, Mann-Whitney test, Red lines at median. **a-d**, COVIDsortium HCW cohort.

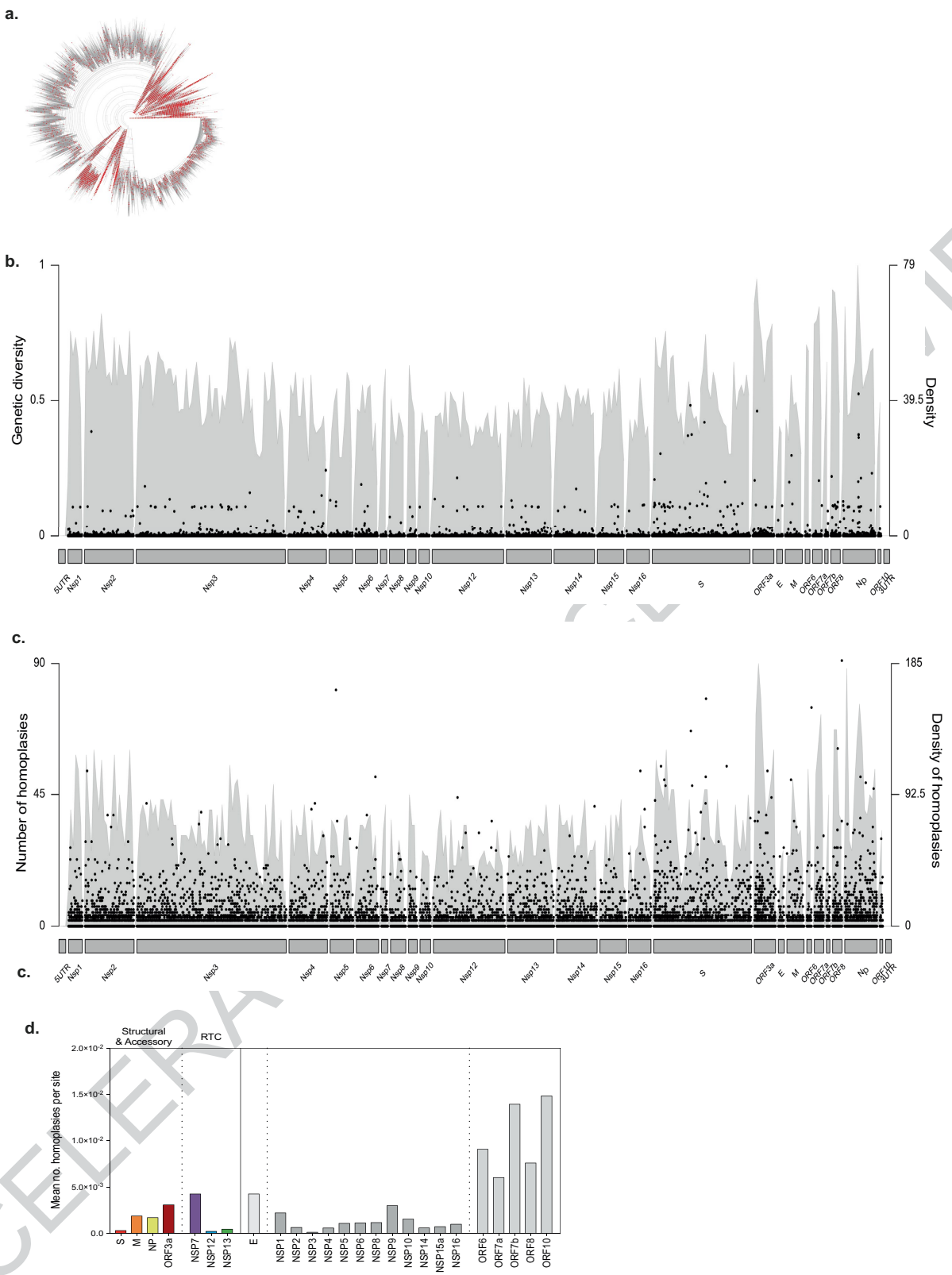

Extended Data Fig. 5 | Diversity along SARS-CoV-2 genome. a, Radial phylogeny of SARS-CoV-2 sequence diversity (611,893 genomes) with the 13,785 accessions subsampled for diversity analysis shown in red. **b**, Genetic diversity (Nei's genetic diversity index) at individual nucleotides along the SARS-CoV-2 genomes, together with the density of polymorphic nucleotides over an 100-nucleotide sliding window shown in grey shading (right y-axis) and **c**, Homoplasies (recurrent mutational emergences) at individual nucleotides, together with the density of the number of homoplasies recorded over an 100-nucleotide sliding window shown in grey shading (right y-axis). **d**, Mean number of homoplasies across a given protein. Viral proteins not assayed for T-cell responses are shown in grey.

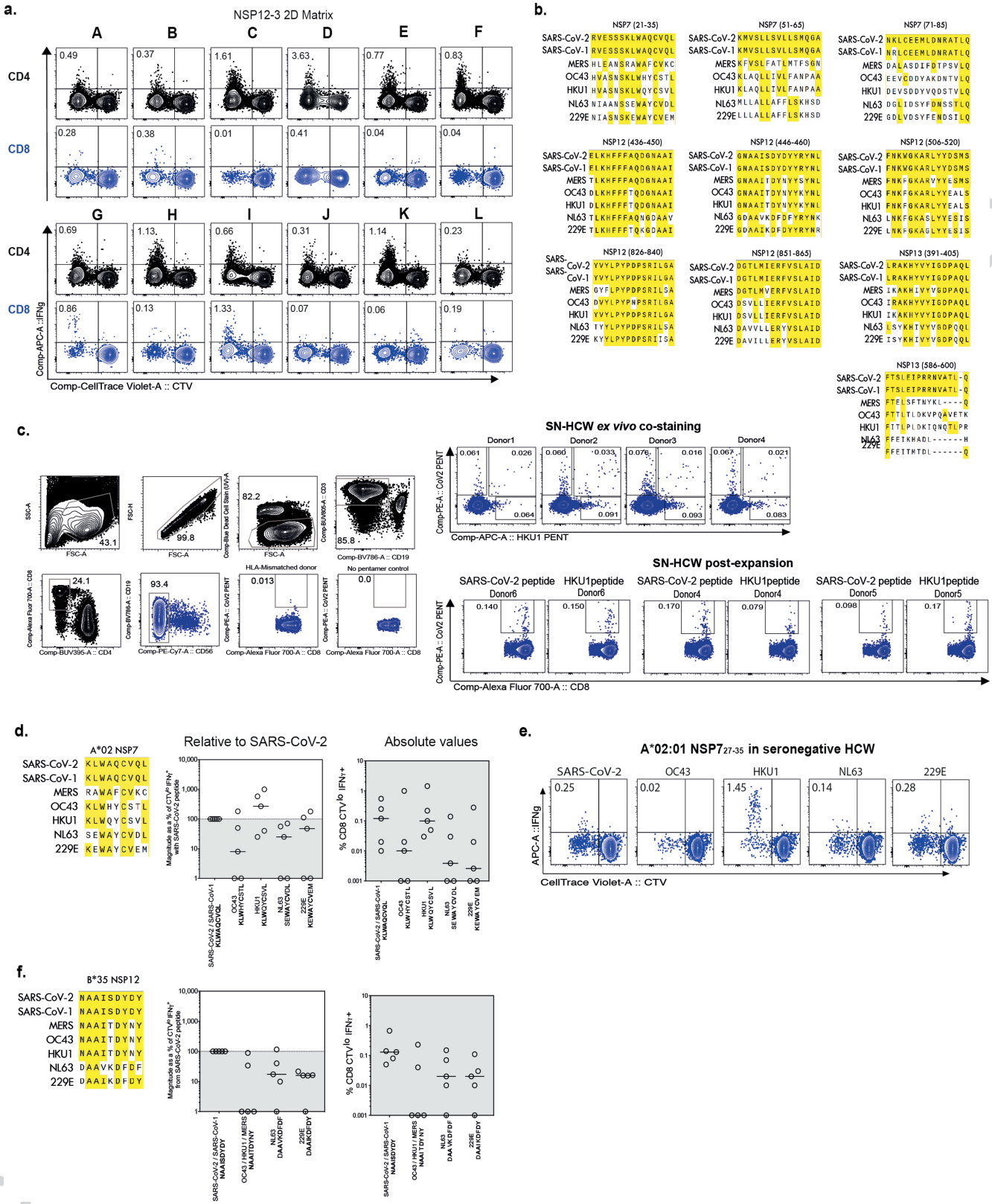

Extended Data Fig. 6 | See next page for caption.

Extended Data Fig 6 | Cross-reactive coronavirus-specific T-cells in seronegative HCW. a, Example 2D-mapping matrix after 10-day expansion with NSP12-3 peptide pool in an SN-HCW (antigen-specific, $CTV^{lo}IFN\gamma+$; percentage of CD4+ or CD8+ shown). **b**, Alignment of *Coronaviridae* consensus sequences at immunogenic 15mers peptides (Extended Data Table 4). Conserved amino acids in yellow. **c**, (left) Example gating (lymphocytes (SSC-A,FSC-A)/singlets(FSC-A,FSC-H)/Live(Live-dead$^-$)/CD3+CD19-/CD8+CD4-/CD56-; example of staining in HLA-mismatched donor and fluorescence minus one for pentamer shown) and (right above) pentamer stains of PBMC from SN-HCW at wk16-26 *ex vivo* (co-staining of pentamers loaded with SARS-CoV-2 peptide KLWAQCVQL and HKU1 peptide KLWQYCSVL) and (right below) after 10-day expansion with SARS-CoV-2 peptide or HKU1 peptide (stained with SARS-CoV-2 peptide loaded pentamer). Percentage of CD8+ shown. **d**, Alignment of *Coronaviridae* sequences at HLA-A*02-restricted epitope in NSP7 (left) and magnitude of CD8+ T-cell response ($CTV^{lo}IFN\gamma+$) after 10-day expansion with HCoV variant sequence peptides as a percentage of response with SARS-CoV-2 sequence peptide (middle) or absolute percentage of total CD8+ (right). **e**, Example plot of CTV vs. IFNγ after 10-day expansion with SARS-CoV-2 or HCoV sequence 9-mer peptides (gated on lymphocytes/singlets/live cells/CD3+/CD56-CD4-/CD8+). **f**, Alignment of *Coronaviridae* sequences at B*035-restricted epitope in NSP12 (left), magnitude of CD8+ T-cell response ($CTV^{lo}IFN\gamma+$) after 10-day expansion with HCoV variant sequence peptides as a percentage of response with SARS-CoV-2 sequence peptide (middle) or absolute percentage of total CD8+ (right). **d,f**, Conserved amino acids in yellow. **d-f**, SN-HCW wk16. **a, c-f**, COVIDsortium HCW cohort. **d-f**, SN-HCW wk16. **d,f**, Lines, median.

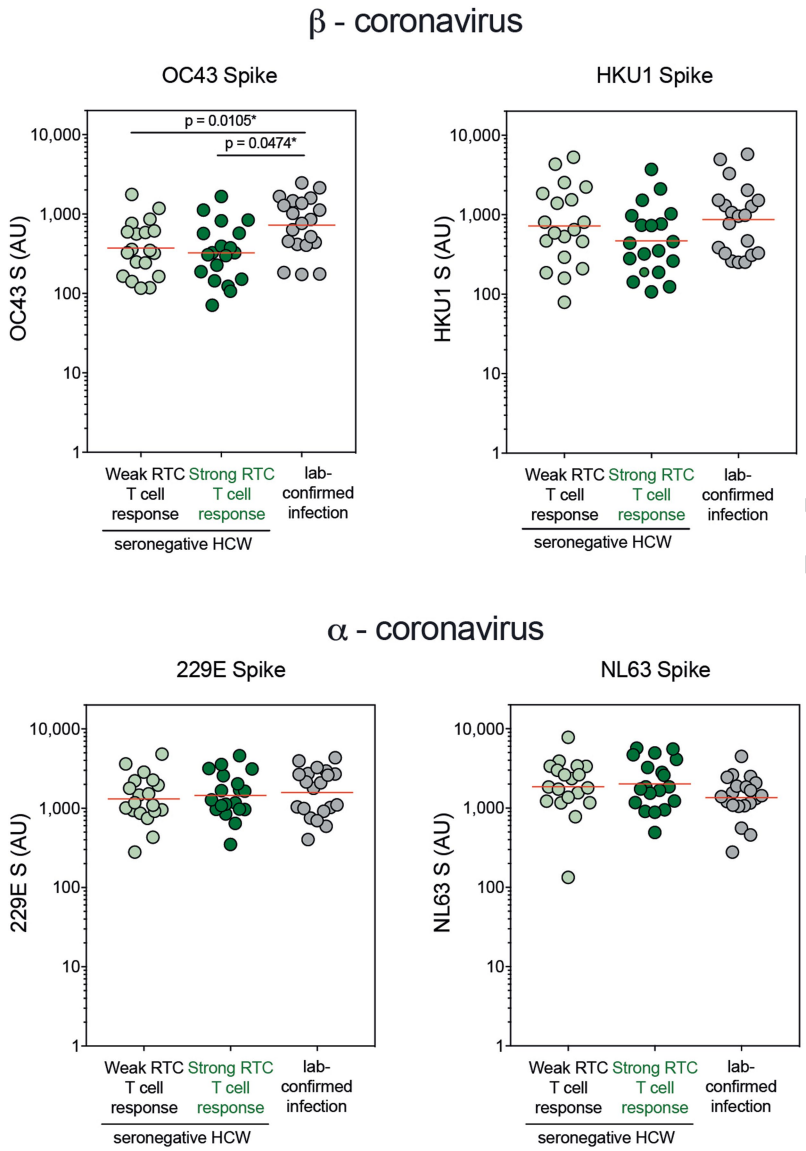

Extended Data Fig. 7 | Anti-spike IgG to human endemic coronaviruses. Anti-spike IgG titres were measured post-infection (wk8, time of peak SARS-CoV-2 S1 IgG seropositivity in COVIDsortium HCW cohort) in HCW with laboratory-confirmed infection (n=20), and post-exposure (wk8) in SN-HCW with weak (<50 SFC/10^6 PBMC, n=19) or strong RTC-specific T-cell response at wk16 (n=19, >50 SFC/10^6 PBMC). Red lines, geomean.

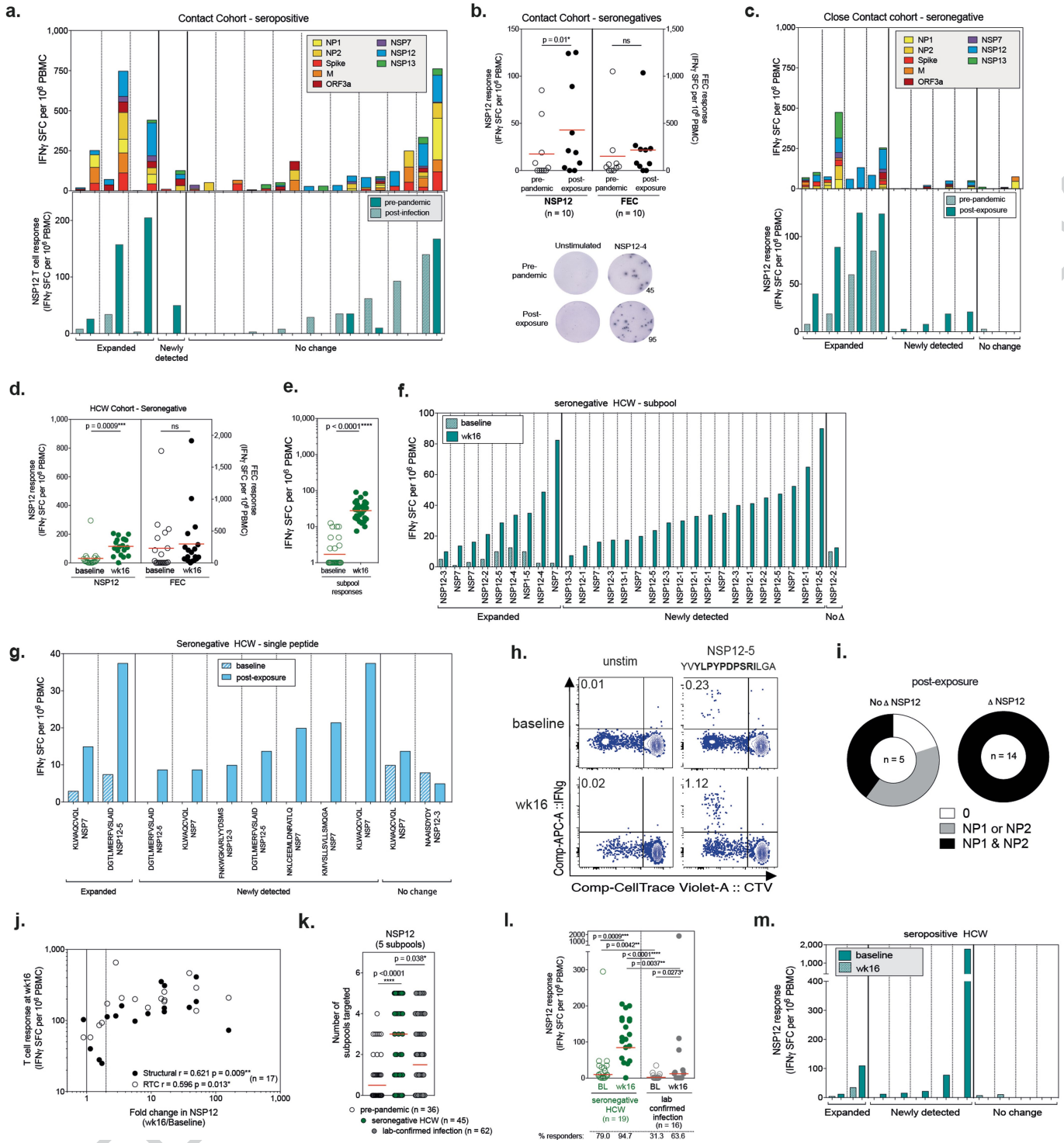

Extended Data Fig. 8 | See next page for caption.

Extended Data Fig. 8 | *In vivo* expansion of pre-existing SARS-CoV-2-reactive T-cells post-infection or post-exposure. a, Change in magnitude of T-cell response between pre-pandemic and post-infection (upper panel: all proteins, lower panel: NSP12) in seropositive close contacts of cases. **b**, Summary data for paired pre-pandemic and post-exposure NSP12 and Flu/EBV/CMV (FEC) responses in seronegative close contacts of infections. Below; example ELISpot well images from a seronegative close contact (NSP12-4: pre-pandemic 45 and post-exposure 95 SFC/10^6 PBMC). **c**, Change in magnitude of T-cell response between pre-pandemic and post-exposure samples (upper panel: all proteins, lower panel: NSP12) from seronegative close contacts of cases. **d**, Summary data for NSP12 and FEC responses in SN-HCW (sub-group with the top RTC response at wk16, n=19, Extended Data Fig. 4a). **e**, Summary data and **f**, change in magnitude of T-cell responses for individual HCW to NSP7 (15 peptide pool) or a single subpool from NSP12 and NSP13 between baseline and post-exposure in SN-HCW (wk16-26, 29 responses from 13 SN-HCW). **g**, Change in magnitude of T-cell response to individual 9-15mer peptides pre- and post-exposure in SN-HCW (wk16-26, 11 responses from 9 SN-HCW). **h**, Example plots of CTV^{lo} $IFN\gamma^+$ SARS-CoV-2-specific T-cells after 10day expansion of PBMC from baseline and wk16 with peptide #166 (YVYLPYPDPSRILGA) or unstimulated in an HLA-B*51+ SN-HCW (gated on CD8+, percentage of CD8+ shown, gating strategy Extended Data Fig. 3a). **i**, Proportion of SN-HCW with NP1 + NP2-reactive T-cells grouped by those with and without newly detected or expanded NSP12 responses at wk16, Fig. 4b. **j**, Correlation between the fold-change in NSP12 between recruitment and wk16 and total response to RTC or structural proteins at wk16 in SN-HCW. Dotted line at 2-fold increase. **k**, The breadth of the NSP12-specific T-cell response (number of subpools recognised, pre-pandemic or wk16). **l** Change in magnitude of the T-cell response to NSP12 between baseline (open circles) and wk16 (closed circles) in SN-HCW and HCW with laboratory-confirmed infection. Percentage of responders shown below. **m**, Change in magnitude of NSP12-specific T-cell response between pre-pandemic and post-infection in HCW with laboratory-confirmed infection. **a,c,f-g,m**, Expanded, >2-fold increase or >35 SFC/10^6 PBMC increase. **a**, Red line mean, **d-e,l**, Red line/bars, geomean. **k**, red line, median. **b,d,e** Wilcoxon test. **l**, Mann-Whitney (unpaired) and Wilcoxon (paired) tests. **k**, Kruskal-Wallis with Dunn's correction. **j**, Spearman r. **a-c**, Contact cohort, Extended Data Table 5. **d-m**, COVIDsortium cohort Extended Data Table 1.

Extended Data Table 1 | Cohort Demographics

	COVIDsortium HCW cohort			Contact Cohort		Pre-pandemic cohorts	
	Total Cohort	Lab-confirmed infection	Seronegatives	Seropositive	Seronegatives	London	Singapore
Number of subjects	731	76	58	13	10	53	12/16*
Mean age (range)	38.1 (18-71)	41.7 (25-62)	37.9 (21-62)	24.9 (20-65)	26.4 (20-32)	26.5 (20-59)	40 (30-59)
Sex:							
Female, n (%)	486 (66.76)	50 (65.79)	36 (62.07)	9 (69.2)	5 (50)	35 (66.04)	4 (33.33)
Male, n (%)	242 (33.34)	26 (34.21)	22 (37.93)	4 (30.8)	5 (50)	18 (33.96)	8 (66.67)
Ethnicity:							
White, n (%)	479 (65.80)	55 (72.37)	41 (70.68)	8 (61.5)	9 (90)	39 (73.58)	2 (16.67)
non-White, n (%)	252 (34.62)	21 (27.63)	17 (29.31)	5 (38.5)	1 (10)	14 (26.42)	10 (83.33)
Recent Travel (pre-March 2020):							
Yes	303 (41.51)	33 (43.42)	26 (44.83)				
COVID-19 Patient Exposure:							
Yes	315 (43.09)	33 (43.42)	17 (29.31)				
COVID-19 Colleague Exposure:							
Yes	218 (29.86)	19 (25.00)	10 (17.24)				
COVID-19 Household Exposure:							
Yes	8 (1.09)	5 (6.58)	0 (0)				
Role:							
Laboratory	12 (1.64)	2 (2.63)	2 (3.45)				
Nurse	231 (31.60)	25 (32.89)	22 (37.93)				
Doctor	150 (20.52)	20 (26.32)	12 (20.69)				
Administration	32 (4.38)	3 (3.95)	2 (3.45)				
Allied Healthcare Professional	185 (25.31)	15 (19.74)	14 (24.14)				
Health Care Assistant	43 (5.88)	2 (2.63)	1 (1.72)				
Other	78 (10.67)	9 (11.85)	5 (8.62)				
Location:							
Laboratory	42 (5.75)	3 (3.95)	6 (10.34)				
Cardiac	108 (14.77)	18 (23.68)	12 (20.69)				
ICU	126 (17.24)	8 (10.53)	7 (12.07)				
Other medical	58 (7.93)	10 (13.16)	6 (10.34)				
Anaesthesia	5 (0.68)	1 (1.32)	1 (1.72)				
A&E	24 (3.28)	2 (2.63)	0 (0)				
Other	361 (49.39)	30 (39.47)	26 (44.83)				
Unspecified	7 (0.96)	4 (5.26)	0 (0)				
Early PPE usage:							
Yes	584 (80.11)	62 (81.58)	39 (67.24)				
Aerosol creating procedures:							
Yes	189 (25.89)	15 (19.74)	13 (22.42)				

	COVIDsortium SN-HCW divided by post-exposure T cell response	
	Seronegatives Weak RTC T cell response (<50 SFU/10^6 PBMC)	Seronegatives Strong RTC T cell response (>50 SFU/10^6 PBMC)
Number of subjects	20	20
Mean age (range)	36.5 (21-58)	43.6 (27-60)
Sex:		
Female, n (%)	13 (65.00)	14 (70.00)
Male, n (%)	7 (35.00)	6 (30.00)
Ethnicity:		
White, n (%)	14 (70.00)	15 (75.00)
non-White, n (%)	6 (30.00)	5 (25.00)
Recent Travel (pre-March 2020):		
Yes	8 (40.00)	10 (50.00)
COVID-19 Patient Exposure:		
Yes	5 (25.00)	6 (30.00)
COVID-19 Colleague Exposure:		
Yes	4 (20.00)	6 (30.00)
COVID-19 Household Exposure:		
Yes	0 (0)	0 (0)
Role:		
Laboratory	0 (0)	2 (10.00)
Nurse	7 (35.00)	8 (40.00)
Doctor	3 (15.00)	5 (25.00)
Administration	0 (0)	1 (5.00)
Allied Healthcare Professional	8 (40.00)	3 (15.00)
Health Care Assistant	0 (0)	0 (0)
Other	2 (10.00)	1 (5.00)
Location:		
Laboratory	2 (10.00)	3 (15.00)
Cardiac	5 (25.00)	3 (15.00)
ICU	1 (5.00)	4 (20.00)
Other medical	3 (15.00)	3 (15.00)
Anaesthesia	1 (5.00)	0 (0)
A&E	0 (0)	0 (0)
Other	2 (10.00)	7 (35.00)
Unspecified	0 (0)	0
Early PPE usage:		
Yes	12 (60.00)	14 (70.00)
Aerosol creating procedures:		
Yes	5 (25.00)	4 (20.00)

A&E, accident and emergency department; ICU, intensive care unit; PPE, personal protective equipment; RTC, replication-transcription complex. * demographics for 4 pre-pandemic samples unknown.

Extended Data Table 2 | T-cell proliferation assay in seronegative HCW

Donor	Week	Antigen	Subpool	Minipool	Peptide	CD4 % CTV-IFNγ+	CD8 % CTV-IFNγ+	% CD4
a	16	Spike/M/ORF3a	-	-	-	0.11%	0.02%	81.78
a	16	FEC	-	-	-	0.00%	10.99%	0.00
a	16	NSP7	-	-	-	0.81%	0.19%	80.96
a	16	NSP12	-	-	-	0.23%	0.01%	95.00
a	16	NSP13	-	-	-	1.04%	0.06%	94.79
a	16	NSP7	-	A	-	0.36%	0.01%	97.81
a	16	NSP7	-	B	-	0.49%	0.01%	98.39
a	16	NSP7	-	C	-	1.23%	0.00%	100.00
a	16	NSP7	-	D	-	0.53%	0.00%	100.00
a	16	NSP7	-	E	-	0.68%	0.00%	99.66
a	16	NSP7	-	F	-	0.49%	0.01%	98.39
a	16	NSP7	-	G	-	1.12%	0.02%	98.50
a	16	NSP7	-	H	-	1.57%	0.01%	99.43
a	16	NSP7	-	C&G	11	0.30%	0.00%	100.00
a	16	NSP7	-	C&H	15	0.11%	0.01%	91.67
a	16	NSP7	-	A&F	5	0.16%	0.06%	72.41
a	16	NSP12	3	B&I	88	0.07%	0.00%	100.00
a	16	NSP7	-	-	5a	-	0.02%	-
a	16	NSP7	-	-	5b	-	0.00%	-
a	16	NSP7	-	-	5c	-	0.05%	-
a	16	NSP7	-	-	5d	-	0.00%	-
a	16	NSP7	-	-	5e	-	0.00%	-
b	16	NSP7	-	-	-	1.14%	0.23%	83.06
b	16	NSP12	3	-	-	2.07%	0.45%	82.06
b	16	NSP13	-	-	-	0.58%	0.04%	94.23
b	16	Spike	-	-	-	0.20%	0.01%	95.92
b	16	NSP12	3	A	-	1.68%	0.31%	84.32
b	16	NSP12	3	B	-	0.38%	0.13%	74.15
b	16	NSP12	3	C	-	0.84%	0.23%	78.32
b	16	NSP12	3	D	-	1.12%	0.26%	81.01
b	16	NSP12	3	E	-	0.77%	0.34%	69.21
b	16	NSP12	3	F	-	1.36%	0.40%	77.16
b	16	NSP12	3	G	-	1.26%	0.20%	86.15
b	16	NSP12	3	H	-	0.67%	0.07%	90.24
b	16	NSP12	3	I	-	1.81%	0.23%	88.62
b	16	NSP12	3	J	-	0.37%	0.29%	55.85
b	16	NSP12	3	K	-	0.60%	0.29%	67.23
b	16	NSP12	3	L	-	0.65%	0.44%	59.50
c	16	FEC	-	-	-	0.07%	8.56%	0.81
c	16	NP	1&2	-	-	0.00%	0.19%	0.00
c	16	NSP7	-	-	-	0.61%	0.08%	88.72
c	16	NSP13	-	-	-	0.30%	0.00%	100.00
c	16	NSP12	1	-	-	0.81%	0.00%	100.00
c	16	NSP12	2	-	-	0.11%	0.06%	65.96
c	16	NSP12	3	-	-	0.62%	0.08%	88.50
c	16	NSP12	3	-	-	0.03%	0.14%	19.54
c	16	NSP12	3	A	-	0.36%	0.26%	57.98
c	16	NSP12	3	B	-	0.24%	0.36%	39.92
c	16	NSP12	3	C	-	1.48%	0.00%	100.00
c	16	NSP12	3	D	-	3.50%	0.39%	89.96
c	16	NSP12	3	E	-	0.64%	0.02%	97.63
c	16	NSP12	3	F	-	0.70%	0.02%	97.02
c	16	NSP12	3	G	-	0.56%	0.84%	39.96
c	16	NSP12	3	H	-	1.00%	0.11%	90.05
c	16	NSP12	3	I	-	0.53%	1.31%	28.78
c	16	NSP12	3	J	-	0.18%	0.05%	78.38
c	16	NSP12	3	K	-	1.01%	0.04%	96.23
c	16	NSP12	3	L	-	0.10%	0.17%	36.85
c	16	NSP12	3	B&G	76	0.05%	0.00%	100.00
c	16	NSP12	3	D&H	84	0.05%	0.00%	100.00
c	16	NSP12	3	B&I	88	0.23%	0.11%	67.84
c	16	NSP12	3	D&K	102	0.08%	0.00%	100.00
c	16	NSP12	5	E&J	171	0.11%	0.03%	76.39
c	16	NSP13	3	D&I	90a	-	0.08%	-
c	16	NSP13	3	D&I	90b	-	0.00%	-
c	16	NSP13	3	D&I	90c	-	0.01%	-
c	16	NSP13	3	D&I	90d	-	0.00%	-
d	16	FEC	-	-	-	0.06%	17.90%	0.33
d	16	NSP7	-	-	-	0.34%	0.03%	90.90
d	16	NSP12	2	-	-	0.41%	0.01%	97.61
d	16	NSP12	3	-	-	0.09%	0.00%	100.00
d	16	NSP12	5	-	-	0.03%	0.16%	16.13
d	16	NSP13	3	-	-	0.33%	0.00%	100.00
d	16	NSP7	-	C&G	11	0.00%	0.03%	0.00
d	16	NSP7	-	C&H	15	0.24%	0.04%	86.02
d	16	NSP12	3	B&I	88	0.00%	0.00%	0.00
d	16	NSP12	3	D&I	90	0.17%	0.00%	97.84
e	16	NSP7	-	A&F	5	0.01%	0.06%	17.65
e	16	NSP7	-	-	-	0.18%	0.12%	60.53
e	16	NSP12	3	I	-	0.01%	0.01%	46.59
e	16	NSP12	3	-	-	0.16%	0.02%	87.70
e	16	NSP12	3	B&I	88	0.02%	0.00%	100.00
e	16	NSP12	3	D&I	90	0.01%	0.00%	100.00
e	16	NSP13	3	D&I	90a	-	0.13%	-
e	16	NSP14	3	D&I	90b	-	0.00%	-
e	16	NSP15	3	D&I	90c	-	0.15%	-
e	16	NSP16	3	D&I	90d	-	0.02%	-

Donor	Week	Antigen	Subpool	Minipool	Peptide	4 % CTV-IFN	8 % CTV-IFN	% CD4
f	29	NSP12	-	-	-	1.47%	0.60%	71.04
f	29	NSP12	5	-	-	0.21%	0.27%	43.98
f	29	NSP13	-	-	-	3.40%	0.04%	98.84
f	29	Spike	-	-	-	0.10%	0.00%	100.00
f	29	NSP12	3	A	-	0.16%	0.41%	28.32
f	29	NSP12	3	B	-	0.18%	0.10%	64.54
f	29	NSP12	3	C	-	0.08%	0.12%	40.59
f	29	NSP12	3	D	-	0.27%	0.25%	52.11
f	29	NSP12	3	E	-	0.28%	0.30%	48.45
f	29	NSP12	3	F	-	0.09%	0.28%	24.73
f	29	NSP12	3	G	-	0.32%	0.00%	100.00
f	29	NSP12	3	H	-	0.17%	0.15%	53.42
f	29	NSP12	3	I	-	0.21%	1.71%	11.03
f	29	NSP12	3	J	-	0.16%	0.06%	72.97
f	29	NSP12	3	K	-	0.27%	0.18%	60.18
f	29	NSP12	3	L	-	0.10%	0.37%	21.61
f	29	NSP12	3	-	-	1.61%	0.00%	100.00
f	29	NSP12	3	I	-	0.13%	0.03%	81.99
f	29	NSP12	3	A&I	87	0.00%	0.00%	100.00
f	29	NSP12	3	B&I	88	0.10%	0.02%	81.30
f	29	NSP12	3	D&I	90	0.17%	0.08%	68.27
f	29	NSP12	3	F&I	92	0.00%	0.00%	0.00
f	29	NSP7	-	A&F	5	0.78%	0.00%	100.00
g	16	Spike	-	-	-	0.19%	0.00%	100.00
g	16	NSP12	2	-	-	0.00%	0.12%	0.00
h	16	NSP12	5	E&J	171	0.17%	0.01%	94.44
h	16	NSP12	3	-	-	0.25%	0.11%	69.83
h	16	NSP13	3	D&I	90a	-	0.14%	-
h	16	NSP13	3	D&I	90b	-	0.00%	-
h	16	NSP13	3	D&I	90c	-	0.00%	-
h	16	NSP13	3	D&I	90d	-	0.03%	-
i	16	NSP7	-	-	-	0.01%	0.13%	7.14
i	16	NSP7	-	A&F	5	0	0.06%	0.00
i	16	NSP7	-	-	5a	-	0.01%	-
i	16	NSP7	-	-	5b	-	0.01%	-
i	16	NSP7	-	-	5c	-	0.10%	-
i	16	NSP7	-	-	5d	-	0.00%	-
i	16	NSP7	-	-	5e	-	0.02%	-
j	16	NSP12	3	-	-	0.59%	0.48%	55.35
j	16	NSP12	3	D&I	90	-	0.62%	-
j	16	NSP12	3	D&I	90a	-	0.67%	-
j	16	NSP12	3	D&I	90b	-	0.23%	-
j	16	NSP12	3	D&I	90c	-	0.07%	-
j	16	NSP12	3	D&I	90d	-	0.11%	-
j	16	NSP12	4	-	148	0.14%	0.10%	58.33
k	4	NSP12	4	-	-	0.09	0.03	75.00
l	16	FEC	-	-	-	0.76%	4.48%	14.50
l	16	NP	1&2	-	-	0.01%	0.01%	38.46
l	16	ORF3a	-	-	-	0.07%	0.52%	11.66
l	16	pike/M/ORF3	-	-	-	0.04%	0.14%	20.56
l	16	NSP7	-	-	5a	-	0.55%	-
l	16	NSP7	-	-	5b	-	1.00%	-
l	16	NSP7	-	-	5c	-	0.22%	-
l	16	NSP7	-	-	5d	-	0.0039	-
l	16	NSP7	-	-	5e	-	0.0026	-
m	16	NSP12	4	-	148	0.10%	0.02%	83.02
m	16	NSP13	3	D&I	90a	-	0.05%	-
m	16	NSP13	3	D&I	90b	-	0.04%	-
m	16	NSP13	3	D&I	90c	-	0.02%	-
m	16	NSP13	3	D&I	90d	-	0.01%	-
n	16	FEC	-	-	-	0.14%	5.33%	2.56
o	16	FEC	-	-	-	5.00%	12.73%	28.20
p	16	NSP7	-	-	5a	-	0.25%	-
p	16	NSP7	-	-	5b	-	0.02%	-
p	16	NSP7	-	-	5c	-	1.45%	-
p	16	NSP7	-	-	5d	-	0.14%	-
p	16	NSP7	-	-	5e	-	0.28%	-
p	16	NSP7	-	-	5a	-	0.21%	-
p	16	NSP7	-	-	5b	-	0.30%	-
p	16	NSP7	-	-	5c	-	0.86%	-
p	16	NSP7	-	-	5d	-	0.36%	-
p	16	NSP7	-	-	5e	-	0.16%	-
p	16	NSP7	-	-	5a	-	0.11%	-
p	16	NSP7	-	-	5b	-	0.01%	-
p	16	NSP7	-	-	5c	-	0.19%	-
p	16	NSP7	-	-	5d	-	0.00%	-
q	16	NSP7	-	-	5a	-	0.12%	-
q	16	NSP7	-	-	5b	-	0.00%	-
q	16	NSP7	-	-	5c	-	0.03%	-
q	16	NSP7	-	-	5d	-	0.03%	-
q	16	NSP7	-	-	5e	-	0	-
r	0	NSP12	5	F&I	166	-	0.22%	-
r	16	NSP12	5	F&I	166	-	1.10%	-

Extended Data Table 3 | SARS-CoV-2 Neis genetic diversity and number of homoplasies per site per gene region

Neis genetic diversity per site, by region

Region	Mean	Median	SD
Nsp3	1.57E-07	0	1.29E-06
Nsp12	**2.69E-07**	**0**	**2.67E-06**
Nsp14	5.34E-07	0	4.38E-06
Nsp2	5.54E-07	7.58E-08	5.49E-06
Nsp13	5.83E-07	0	4.17E-06
S	5.98E-07	0	4.95E-06
Nsp15	7.88E-07	0	6.60E-06
Nsp4	7.92E-07	0	6.60E-06
Nsp16	8.13E-07	0	7.30E-06
Nsp8	8.50E-07	0	6.42E-06
Nsp5	8.64E-07	0	7.95E-06
Nsp10	1.21E-06	0	1.30E-05
Nsp6	1.32E-06	0	1.00E-05
Nsp7	1.80E-06	0	5.78E-06
Nsp1	1.95E-06	2.69E-07	1.33E-05
M	2.20E-06	0	2.23E-05
ORF3a	3.03E-06	1.75E-07	2.34E-05
NP	3.30E-06	1.15E-07	2.25E-05
Nsp9	3.32E-06	0	2.22E-05
ORF6	3.92E-06	7.80E-07	1.96E-05
E	4.40E-06	0	3.76E-05
ORF7a	4.63E-06	4.02E-07	3.46E-05
ORF8	1.25E-05	3.97E-07	5.71E-05
ORF10	1.55E-05	1.25E-06	9.08E-05
ORF7b	1.59E-05	1.10E-06	7.32E-05

No. Homoplasies per site, by region

Region	Mean	Median	SD
Nsp3	0.000175932	0	0.000519326
Nsp12	**0.000258192**	**0**	**0.000952715**
S	0.000353033	0	0.001182173
Nsp13	0.000502952	0	0.001535093
Nsp4	0.000630667	0	0.002027798
Nsp14	0.000635312	0	0.001918301
Nsp2	0.000687067	0	0.001911003
Nsp15	0.000774054	0	0.002450595
Nsp16	0.001038492	0	0.004017116
Nsp5	0.001132043	0	0.004471706
Nsp6	0.001173207	0	0.003966735
Nsp8	0.001218697	0	0.004520017
Nsp10	0.001598721	0	0.004885641
NP	0.001747292	0	0.004215111
M	0.00192376	0	0.006486963
Nsp1	0.002253086	0	0.005686097
Nsp9	0.00304557	0	0.0080396
ORF3a	0.003140388	0	0.00685446
Nsp7	0.004306382	0	0.011129816
E	0.004309018	0	0.01490037
ORF7a	0.006074296	0	0.012362245
ORF8	0.007651766	0	0.021193027
ORF6	0.009134004	0	0.034665426
ORF7b	0.014003673	0	0.030034154
ORF10	0.014902476	0	0.036781834

Neis genetic diversity per site, pairwise comparison to Nsp12

Region	*p*	*p.adj*	*p.format*	Significance
ORF3a	5.29E-63	1.60E-60	<2E-16	****
NP	1.17E-46	3.50E-44	<2E-16	****
ORF8	2.74E-45	8.20E-43	<2E-16	****
ORF7a	2.88E-38	8.50E-36	<2E-16	****
S	1.78E-18	4.40E-16	<2E-16	****
Nsp2	2.45E-40	7.30E-38	<2E-16	****
Nsp1	1.75E-20	4.50E-18	<2E-16	****
Nsp3	5.96E-19	1.50E-16	<2E-16	****
ORF6	2.76E-14	6.50E-12	2.80E-14	****
ORF7b	1.22E-12	2.80E-10	1.20E-12	****
ORF10	1.15E-08	2.30E-06	1.10E-08	****
Nsp14	3.29E-05	5.10E-03	3.30E-05	****
Nsp4	1.45E-04	2.10E-02	0.00014	***
Nsp15	4.16E-04	5.90E-02	0.00042	***
Nsp6	4.87E-04	6.80E-02	0.00049	***
Nsp13	3.76E-03	4.80E-01	0.00376	**
Nsp7	5.89E-03	7.10E-01	0.00589	**
M	1.39E-02	1.00E+00	0.01388	*
Nsp9	1.40E-02	1.00E+00	0.01396	*
Nsp5	3.12E-02	1.00E+00	0.03125	*

Pairwise differences are assessed following wilcoxon test.

No. Homoplasies per site, pairwise comparison to Nsp12

Region	*p*	*p.adj*	*p.format*	Significance
NP	2.69E-08	8.10E-06	2.70E-08	****
ORF3a	4.84E-08	1.40E-05	4.80E-08	****
ORF8	1.11E-04	3.20E-02	0.00011	***
S	1.41E-04	4.10E-02	0.00014	***
ORF7a	4.22E-03	1.00E+00	0.00422	**
ORF7b	1.57E-02	1.00E+00	0.01565	*
Nsp14	2.51E-02	1.00E+00	0.02505	*

Extended Data Table 4 | Immunogenic peptides recognised by CD4+ or CD8+ T-cells in seronegative HCW

	Protein (amino acid residues)	SARS-CoV-2 amino acid sequence	MHC restriction (predicted)
CD4	**NSP7 (21-35) #5**	RVESSSKLWAQCVQL	-
	NSP7 (51-65) #11	KMVSLLSVLLSMQGA	-
	NSP7 (71-85) #15	NKLCEEMLDNRATLQ	-
	NSP12 (436-450) #88	ELKHFFFAQDGNAAI	-
	NSP12 (446-460) #90	GNAAISDYDYYRYNL	-
	NSP12 (506-520) #102	FNKWGKARLYYDSMS	-
	NSP12 (851-865) #171	DGTLMIERFVSLAID	-
	NSP13 (391-405) #79	LRAKHYVYIGDPAQL	-
	NSP13 (586-600) #118	FTSLEIPRRNVATLQ	-
CD8	**NSP7 (21-35) #5**	RVESSS**KLWAQCVQL**	A*02:01
	NSP12 (436-450) #88	ELKHFF**FAQDGNAAI**	(A*24:02)
	NSP12 (446-460) #90	G**NAAISDYDY**YRYNL	(B*35:01)
	NSP12 (826-840) #166	YV**YLPYPDPSRI**LGA	B*51:01
	NSP13 (391-405) #79	LRAKHY**VYIGDPAQL**	A*24:02, C*07:01
	NSP13 (586-600) #118	FTSLE**IPRRNVATL**Q	B*07:02, B*08:01

Extended Data Table 5 | Demographics and sampling of Close Contact medical student/laboratory staff cohort

	Serostatus/PCR	Gender	Age (post exposure sample)	Exposure	NSP12 Response	Post-exposure sample: Months since known exposure/PCR+ or symptoms
Close contact	Seronegative	F	20-24	Household Contact	-	8-9
	Seronegative	M	20-24	Suspected household contact*	Expanded	8-9
	Seronegative	M	20-24	Close Contact	Newly Detected	7-8
	Seronegative	F	20-24	Suspected household contact*	Newly Detected	6-7
	Seronegative	M	20-24	Suspected household contact*	Newly Detected	9-10
	Seronegative	F	20-24	Close Contact	Expanded	9-10
	Seronegative	F	20-24	Household Contact	Newly Detected	9-10
	Seronegative	M	20-24	Close Contact	Expanded	8-9
	Seronegative	M	65-69	Household Contact	Expanded	7-8
	Seronegative	F	25-29	Household Contact	-	6-7
Lab-confirmed infection	Seropositive	M	20-24	not known	-	9-10
	Seropositive	F	20-24	Household Contact	-	2-3
	Seropositive	F	20-24	Close Contact	-	9-10
	Seropositive	F	20-24	Suspected household contact*	-	9-10
	PCR+ Seropositive	F	20-24	Close Contact	Newly Detected	2-3
	PCR+ Seropositive	M	20-24	Close Contact	Expanded	1-2
	Seropositive	F	20-24	Close Contact	Expanded	9-10
	PCR+ Seropositive	F	20-24	Household Contact	-	1-2
	Seropositive	F	25-29	not known	Expanded	4-5
	Seropositive	M	25-29	Household Contact	-	5-6
	Seropositive	F	25-29	not known	-	4-5
	PCR+ Seropositive	F	30-34	Occupational	-	1-2
	PCR+ Seropositive	M	25-29	not known	-	1-2

*Household contact with case-defining symptoms but no PCR confirmation available early 2020. Expanded = >2 fold or >35 SFU/10^6 PBMC increase in NSP12 response from pre-pandemic to post-exposure or infection time point.

nature research

Corresponding author(s): Mala Maini, Leo Swadling

Last updated by author(s): Oct, 1 2021

Reporting Summary

Nature Research wishes to improve the reproducibility of the work that we publish. This form provides structure for consistency and transparency in reporting. For further information on Nature Research policies, see Authors & Referees and the Editorial Policy Checklist.

Statistics

For all statistical analyses, confirm that the following items are present in the figure legend, table legend, main text, or Methods section.

n/a	Confirmed
☐	☒ The exact sample size (*n*) for each experimental group/condition, given as a discrete number and unit of measurement
☐	☒ A statement on whether measurements were taken from distinct samples or whether the same sample was measured repeatedly
☐	☒ The statistical test(s) used AND whether they are one- or two-sided *Only common tests should be described solely by name; describe more complex techniques in the Methods section.*
☒	☐ A description of all covariates tested
☐	☒ A description of any assumptions or corrections, such as tests of normality and adjustment for multiple comparisons
☐	☒ A full description of the statistical parameters including central tendency (e.g. means) or other basic estimates (e.g. regression coefficient) AND variation (e.g. standard deviation) or associated estimates of uncertainty (e.g. confidence intervals)
☐	☒ For null hypothesis testing, the test statistic (e.g. *F*, *t*, *r*) with confidence intervals, effect sizes, degrees of freedom and *P* value noted *Give P values as exact values whenever suitable.*
☒	☐ For Bayesian analysis, information on the choice of priors and Markov chain Monte Carlo settings
☒	☐ For hierarchical and complex designs, identification of the appropriate level for tests and full reporting of outcomes
☒	☐ Estimates of effect sizes (e.g. Cohen's *d*, Pearson's *r*), indicating how they were calculated

Our web collection on statistics for biologists contains articles on many of the points above.

Software and code

Policy information about availability of computer code

Data collection	A complete masked alignment was downloaded from the GISAID EpiCoV database on 26/7/2021 together with a GISAID Audacity phylogeny comprising 611,893 accessions. The alignment was subsampled to include 800 of each defined NextStrain phylogenetic clade, as provided by GISAID metadata. For clades containing less than 800 accessions all representatives of that clade were included resulting in a comprehensive sampling over the global phylogeny of 13,785 accessions encompassing the genomic diversity of SARS-CoV-2 to date (Supplementary Table 4, Extended Data Fig. 5).
Data analysis	Software used for data/statistical analysis: FlowJo v.10.7.1; FACSDIVA v9.0; Prism 7.0e and 9.0; Excel v.16.16.09; R version 3.5.3 with RStudio Version 1.0.153 for Mac. Custom scripts used to perform the homology searches, heatmap visualisation and permutation testing are hosted on GitHub (https://github.com/cednotsed/tcell_cross_reactivity_covid.git). Correlogram was produced using corrplot in R (https://github.com/taiyun/corrplot). Polyfunctionality was visualised using SPICE (version 6.0) and pestle (version 2.0), available at https://niaid.github.io/spice/. MUSCLE algorithm with default parameters and percentage identity was calculated in Geneious Prime 2020.1.2. Alignment figures were made in Snapgene 5.1 (GSL Biotech).

For manuscripts utilizing custom algorithms or software that are central to the research but not yet described in published literature, software must be made available to editors/reviewers. We strongly encourage code deposition in a community repository (e.g. GitHub). See the Nature Research guidelines for submitting code & software for further information.

Data

Policy information about availability of data

All manuscripts must include a data availability statement. This statement should provide the following information, where applicable:

- Accession codes, unique identifiers, or web links for publicly available datasets
- A list of figures that have associated raw data
- A description of any restrictions on data availability

All data analysed during this study are included in this published article (and its supplementary information files). Genomic data analysed was obtained from the publicly available NCBI Virus database and, following registration, from the GISAID EpiCoV repository (full list and metadata available at: 10.6084/m9.figshare.16607423). The datasets generated during and/or analysed during the current study are available from the corresponding author on reasonable request. Correspondence and requests for materials should be addressed to MKM or LS.

Protein sequences for SARS-CoV-2 ORF1ab (accession numbers: QHD43415.1, NP_828849.2, YP_009047202.1, YP_009555238.1, YP_173236.1, YP_003766.2 and NP_073549.1) and for HCoV (accessions listed in Supplementary Table 1, NCBI Virus using 245 the taxid: 1118 together with accompanying metadata) were downloaded from the NCBI database (https://www.ncbi.nlm.nih.gov/).

Field-specific reporting

Please select the one below that is the best fit for your research. If you are not sure, read the appropriate sections before making your selection.

☒ Life sciences ☐ Behavioural & social sciences ☐ Ecological, evolutionary & environmental sciences

For a reference copy of the document with all sections, see nature.com/documents/nr-reporting-summary-flat.pdf

Life sciences study design

All studies must disclose on these points even when the disclosure is negative.

Sample size	Sample sizes are given for each figure throughout the paper when individual dots are not shown. Power calculations were performed prior to week 16 sub-study sampling to determine the sample size needed to test the hypothesis that HCW with pre-existing T cell responses are enriched in exposed uninfected group at a range of incidence of infection, assuming 50% of cohort had pre-existing T cell responses. Sample sizes of 18-64 per group were estimated. An age, sex and ethnicity matched nested substudy was designed within the larger (n=731) parent study and 129 attended for 16 week sampling including high volume PBMC isolation. Sample size can vary across figure panels depending on which stimulations were performed (limited by number of PBMC recovered). Cohort sizes given in Figure 1a.
Data exclusions	Classification of HCW and study participants into cohorts is defined in methods as are any specific exclusions of data points from individual graphs. Two HCW in the seronegative cohort (negative for NP and S1 antibodies wk 0-16) had nAb titres just above the threshold IC50 of 50 were excluded from further analyses (exclusion criteria not pre-established, determined using unexposed pre-pandemic and PCR+ samples). No other HCW or individual samples were excluded after data was generated.
Replication	Replication for each assay are described in the methods. Briefly, per sample unstimulated controls were run in duplicate for ELISpot data with no data excluded due to outliers. Due to limited sample availability ELISpots were only repeated on a small number of pre-pandemic samples. Replicates were successful. CTV proliferation assays were repeated and experimental replicates performed on a subset of individuals successfully. Duplicates were used for S1 ELISAs with no outliers excluded. qPCR was repeated on a subset of individuals successfully. Neutralization assays were preformed over a wide range of dilutions in duplicate.
Randomization	Experiments were performed with protocols optimised to reduce batch variation and to ensure mixing of experimental groups across batches e.g Flow cytometer parameters were consistent between runs (No MFI comparisons were performed, only gating and percentage of parent). Samples from pre-pandemic, seronegative HCW and seropositive HCW were ran in parallel on ELISpot plates. Laboratory-confirmed infection was determined by weekly nasopharyngeal RNA stabilizing swabs and reverse transcriptase polymerase chain reaction (RT-PCR; Roche cobas SARS-CoV-2 test, Envelope [E] gene) and antibody assay positivity (Spike protein 1 IgG Ab assay, EUROIMMUN) and anti-nucleocapsid total antibody assay (ROCHE). The seronegative health care worker group were matched for demographics and exposure to the laboratory-confirmed infected group and was defined by negativity by these three tests at all 16 time points as well as negative for neutralising antibodies at week 16 and at selected prior time points as indicated. Unexposed pre-pandemic samples were not matched for demographics (Demographics given in Extended Data Table 1). 'Close-contact cohort' self-identified as having had close contact (household contact or alert by NHS test-and-trace app of close contact with a confirmed case) were divided into seropositive or seronegative (determined by S1 ELISA), Extended Data Table 4.
Blinding	IFNg-ELISpot assays were performed on HCW cohorts prior to unblinding of group (laboratory-confirmed-infection or seronegative). Other experiments were not randomized and the investigators were not blinded to allocation during experiments and outcome assessment, however, experimental set-up and controls ensured accurate replication across technical replicates (see above and methods).

Reporting for specific materials, systems and methods

We require information from authors about some types of materials, experimental systems and methods used in many studies. Here, indicate whether each material, system or method listed is relevant to your study. If you are not sure if a list item applies to your research, read the appropriate section before selecting a response.

Materials & experimental systems

n/a	Involved in the study
☐	☒ Antibodies
☒	☐ Eukaryotic cell lines
☒	☐ Palaeontology
☒	☐ Animals and other organisms
☐	☒ Human research participants
☐	☒ Clinical data

Methods

n/a	Involved in the study
☒	☐ ChIP-seq
☐	☒ Flow cytometry
☒	☐ MRI-based neuroimaging

Antibodies

Antibodies used

Detailed information regarding all antibodies and other fluorescent agents used in this study are listed in the methods with manufacturer, clone, and dilution used.
ELISpot - human anti-IFNγ Ab (1-D1K, Mabtech; 10 µg/ml), biotinylated IFN-γ detection antibody (7-B6-1, Mabtech; 1µg/ml).

FACS: Memory B cell Panel: CD3 Bv510 (Biolegend, clone OKT3, 1:200), CD11c FITC (BD Biosciences, clone B-ly6, 1:100), CD14 Bv510 (Biolegend, clone M5E2, 1:200), CD19 Bv786 (BD bioscience, clone HIB19, 1:50), CD20 AlexFluor700 (BD biosciences 2H7, 1:100), CD21 Bv711 (BD biosciences, clone B-ly4, 1:100), CD27 BUV395 (BD biosciences, clone L128, 1:100), CD38 Pe-CF594 (BD biosciences, clone HIT2, 1:200), IgD Pe-Cy7 (BD biosciences, clone IA6-2, 1:100).

FACS: CTV assay: IL-2 PerCp-eFluor710 (Invitrogen, clone MQ1-17H12, 1:50), TNFα FITC (BD bioscience, clone MAb11, 1:100), CD8α BV785 (Biolegend, clone RPA-T8, 1:200), IFN? BV605 (BD biosciences, clone B27, 1:100), IFN? APC (Biolegend, clone 4S.B3, 1:50), CD3 BUV805 (BD biosciences, clone UCHT1, 1:200), CD4 BUV395 (BD biosciences, clone SK3, 1:200), CD154 (CD40L) Pe-Cy7 (Biolegend, clone 24-31, 1:50), MIP-1-β PE (BD biosciences, clone D21-1351, 1:100).

FACS:MHC class I pentamer panel: CD3 BUV805 (BD biosciences, clone UCHT1, 1:200), CD4 BUV395 (BD biosciences, clone SK3, 1:200), CD56 Pe-Cy7 (BD biosciences, NCAM16.2, 1:100), CD8α Alexa700 (Biolegend, RPA-78, 1:200), post-expansion CD19 Bv786 (BD biosciences, HIB19, 1:100).

Validation

All antibodies and MHC class I pentamers were purchased from well established manufacturers and were validated by the vendor for species and target. e.g. BD biosciences, Biolegend, and Invitrogen antibodies are tested in Knock-out/knock-in primary model systems to ensure biological accuracy in ISO 9001 certified facilities. Side-by-side lot comparisons are performed. Details of antibody clones have been included for cross-referencing of manufacturing company specification/validation processes. We further validated antibodies by titration to optimal concentrations and by using positive controls where possible (e.g. using populations known to express a certain marker or by polyclonal stimulation). MHC class I pentamers were tested in HLA-mismatched individuals to assess background staining and on T cell clones expanded with cognate peptide.

Fluorescence minus one stains were used to define gates in Flowjo for all FACS assays . Positive (SARS-CoV-2 laboratory-confirmer infected) and negative controls (unexposed pre-pandemic samples) were included in each run for memory B cell staining. Positive control wells were used in CTV stains to ensure accurate staining of cytokines and CTV staining was checked on day 0 before stimulation. Unstimulated control wells treated as peptide wells (e.g. addition of DMSO) were run per biological sample for CTV proliferation assays and ELISpots (in duplicate for ELISpots) and all data is presented as background subtracted as described in the methods.

Human research participants

Policy information about studies involving human research participants

Population characteristics

Age, sex and ethnicity of cohorts are provided in Extended Data Table 1 and 4, and in detail for the COVIDsortium in Augusto et al Wellcome Open Research 2020. Substudy recruitment for all wk16 data presented was performed on a cohort of seronegative HCW matched for age, sex, and ethnicity with a group of laboratory-confirmed infected HCW.

Recruitment

Recruitment is described in details in Augusto et al Wellcome Open Research and in the methods section. Adult (>18 years) hospital HCWs who were fit and well to attend work in any role and across a range of clinical areas, were invited to participate via hospital email, posters, staff meetings, training sessions and participant information leaflets (see https://covid-consortium.com). No other inclusion or exclusion criteria were considered.The “COVID-19 Immune Protection and Pathogenesis in Healthcare Worker Bioresource” (NCT04318314) uses a prospective cohort design (Figure 1). The study consists of questionnaires and biological samples (blood samples, nasal swabs ± saliva) performed at all visits: baseline, weekly follow-ups for 15 weeks, and visits at 6 and 12 months. An age, sex and ethnicity matched nested sub-study was designed within the larger (n=731) parent study and 129 attended for 16-week sampling including high volume PBMC isolation. For the 'close-contact cohort' medical students previously enrolled in a BCG vaccine trial (UCL Ethics Project ID Number: 13545/001) were invited to participate by email and were re-consented.

Ethics oversight

The COVIDsortium bioresource was approved by the ethical committee of UK National Research Ethics Service (20/SC/0149) and registered on ClinicalTrials.gov (NCT04318314). The cohort of medical students and laboratory staff was approved by UCL Ethics (Project ID Number: 13545/001) and pre-pandemic healthy donor samples were collected and cryopreserved before August 2019 under ethics numbers 11/LO/0421. All subjects gave written informed consent and the study conformed to the principles

of the Helsinki Declaration.

Note that full information on the approval of the study protocol must also be provided in the manuscript.

Clinical data

Policy information about clinical studies

All manuscripts should comply with the ICMJE guidelines for publication of clinical research and a completed CONSORT checklist must be included with all submissions.

Clinical trial registration	ClinicalTrials.gov (NCT04318314)
Study protocol	ClinicalTrials.gov (NCT04318314), Augusto et al Wellcome Open Research 2020.
Data collection	Data collection is described in detail in Augusto et al Wellcome Open Research and in the methods section. The "COVID-19 Immune Protection and Pathogenesis in Healthcare Worker Bioresource" (NCT04318314) uses a prospective cohort design. The study consists of questionnaires and biological samples (blood samples, nasal swabs ± saliva) performed at all visits: baseline, weekly follow-ups for 15 weeks, and visits at 6 and 12 months. Recruitment was initially at St Bartholomew's Hospital, London, UK (400 HCWs recruited between 23rd and 31st March 2020, just before the peak of new daily cases in London, which happened on the 2nd April, with 1,022 new cases confirmed). To improve statistical power for downstream analyses, we expanded the target sample size to n=1,000 and extended recruitment on 17th April 2020 to other local sites: Royal Free NHS Hospital Trust (large teaching hospital with specialist expertise in infectious diseases). Baseline: Participants complete a baseline questionnaire including standard variables related to demographics and exposures. These included occupation, household details, smoking status, physical activity, anthropometry, medical history (including vaccination history, current medication and dietary supplements), occupational exposure (including specific clinical areas and access to/use of personal protective equipment [PPE]), travel history, previous COVID-19 symptoms, proven contact with SARS-CoV-2 infected individuals, and any prior testing for SARS-CoV-2 infection. Follow-up: Following recruitment (baseline visit), if fit and well to attend work, participants would undertake in-person weekly questionnaires using research electronic data infrastructure (REDCap v8.5.22)16 to capture occupational metadata, new SARS-CoV-2 exposure, symptoms and test results, and biosample collection.
Outcomes	Prospective HCW study. Not applicable

Flow Cytometry

Plots

Confirm that:

☒ The axis labels state the marker and fluorochrome used (e.g. CD4-FITC).

☒ The axis scales are clearly visible. Include numbers along axes only for bottom left plot of group (a 'group' is an analysis of identical markers).

☒ All plots are contour plots with outliers or pseudocolor plots.

☒ A numerical value for number of cells or percentage (with statistics) is provided.

Methodology

Sample preparation	Detailed sample preparation is given in methods. All FACS was performed on frozen and thawed PBMC isolated by density gradient separation. Peripheral blood mononuclear cells (PBMC) were isolated from heparinized blood samples using Pancoll (Pan Biotech) or Histopaque®-1077 Hybri-MaxTM (Sigma-Aldrich) density gradient centrifugation in SepMate tubes (StemCell) according to the manufacturer's specifications. Isolated PBMCs were cryopreserved in fetal calf serum (FCS) containing 10% DMSO and stored in liquid nitrogen.
Instrument	BD biosciences LSRII and Fortessa-X20 flow cytometers.
Software	FACS DIVA version 9.0 was used on instrument and exporting .fcs files were analysed in FlowJo version 10.7.1 (TreeStar)
Cell population abundance	PBMC were stained and run without sorting or enrichment.
Gating strategy	Example gating strategy for CTV proliferation and mapping FACS experiments is given in Extended Data Figure 3a. Example plots are given in Fig. 2c, Fig 3g, and Extended Data Fig 3d and Extended Data Fig. 6a. Data is reported as a percentage of lymphocytes/singlets/live/CD3+/CD4+ or CD8+ defining antigen specificity by production of IFNg and CTV dilution. For memory B cell stains example plots are given in Extended Data Figure 1b and details of cutoff and assay validation are given in Jeffery-Smith et al BioRxiv 2021. Gating is described in legends: MBC expressed as a percentage of lymphocytes, singlets, Live, CD3-CD14-CD19+, CD20+, excluding CD38hi, IgD+ and CD21+CD27- fractions. MHC class I Pentamer gating and example plots in Extended Data Figure 6c.

☒ Tick this box to confirm that a figure exemplifying the gating strategy is provided in the Supplementary Information.